Towards prevention and prediction of infectious diseases with virus sterilization using ultraviolet light and low-temperature plasma and bio-sensing devices for health and hygiene care

Shinya Kumagai,¹ Chikako Nishigori,² Tetsuya Takeuchi,¹ Peter Bruggeman,³ Keisuke Takashima,⁴ Hideki Takahashi,⁴ Toshiro Kaneko,⁴ Eun Ha Choi,⁵ Kazuo Nakazato,^{6,7} Makoto Kambara,⁸ and Kenji Ishikawa^{7,*}

- 1 Meijo University, Japan
- 2 Kobe University, Japan
- 3 University of Minnesota, USA
- 4 Tohoku University, Japan
- 5 Kwangwoon University, Korea
- 6 BioCMOS, Japan
- 7 Nagoya University, Japan
- 8 University of Tokyo, Japan
- *Correspondence ishikawa.kenji@nagoya-u.jp

ABSTRACT

Inspired by the ideas of many authors, we provide insight on state-of-the-art potential technologies for the prevention and prediction of infectious diseases before they spread. This review also surveys virus sterilization with ultraviolet light and low temperature plasma technologies. Researchers in the various fields of medicine, materials, electronics, and plasma sciences have addressed increasingly challenging demands and the discussion encompasses the major challenges in societies that are faced with the threat of infectious diseases. In addition, technologies that use nanomaterials are evaluated for infection prevention and hygiene purposes. Advances in biomedical diagnostics for health care in terms of complementary metal-oxide-semiconductor transistors (CMOS)-based devices and telemetry for health monitoring are also reviewed.

1. Introduction

Since the COVID-19 pandemic caused by the coronavirus SARS-CoV-2 (Severe Acute Respiratory Syndrome Coronavirus-2), daily life around the world has been completely transformed. SARS-CoV-2 is a highly infectious agent that causes potentially fatal respiratory illness and is thus of great global public health concern [1]. The wearing of masks, use of hand sanitizer, and social distancing have become daily routines to reduce the risk of virus transmission during this pandemic [1]. The Japanese campaign of avoiding the 3Cs (closed spaces, crowded places, and close-contact settings) has become a cornerstone of combating the pandemic [2].

The human race has historically been faced with a number of pandemics, such as the Plague and the Spanish flu, which were respectively caused by a bacterium pathogen (*Yersinia pestis*) and H1N1 influenza virus [3]. While the understanding of pathogens in those days was insufficient to stop these pandemics, the continued scientific and technological developments of the 21st century have given us the tools to combat the COVID-19 pandemic.

In this review, we explore how technological advances in plasma, nanotechnology, and semiconductor devices can contribute to the fight against infectious diseases (Fig. 1). The solutions explored cover a variety of areas, which include sterilization of the source of infection, prevention of infections, and the prediction of infectious diseases before they can spread. To enable continued and rapid progress in such technologies, we envision the need for highly collaborative research, particularly the combination of plasma, nitride semiconductors, nanomaterials, and biotechnology (Fig. 2). We discuss possible directions to contribute to solving such global infection problems.

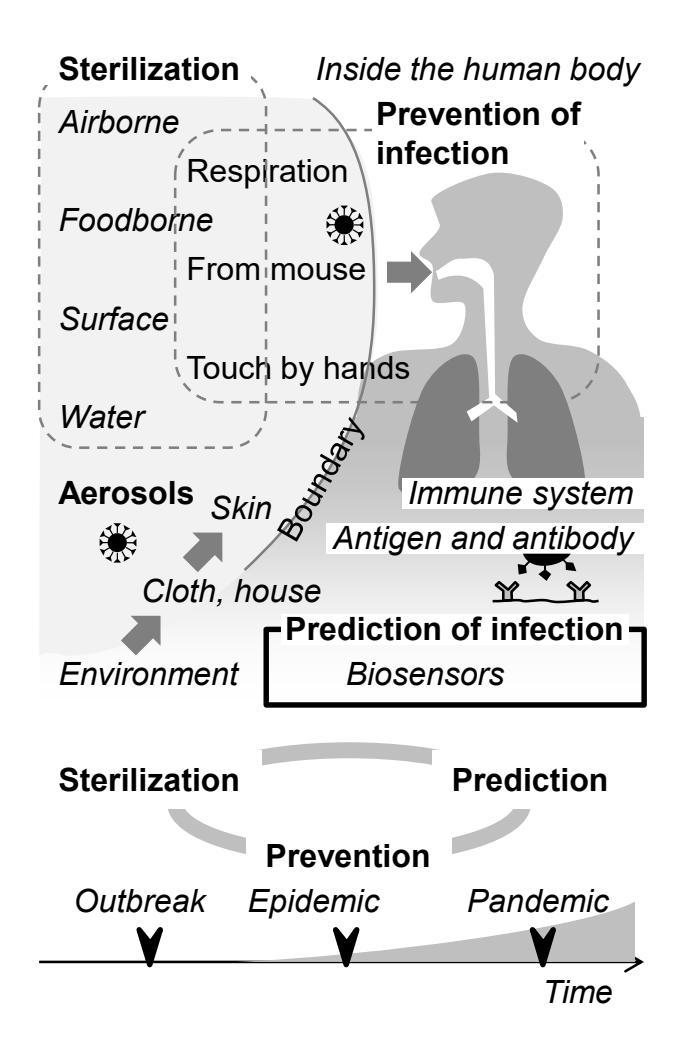


Figure 1. This review covers technological areas of low-temperature plasma, nanotechnologies, and semiconductor devices for solutions to overcome infectious diseases. Decontamination of airborne viruses in aerosols and surface viruses of decontaminated routes could be employed at any time.

How to prevent and predict infectious disease before they spread

Sterilization of viral pathogens

UV lamps, Deep UV LEDs Low-temperature plasma

Reactive O and N species (RONS) UV+RONS, + water (humidity) Short-lived species (radicals)

Prevention: Virus sensing/detection

Membrane filtration (biopsy) Antiviral coating (copper, etc.) Nanomaterials (amperometric) BioCMOS (potentio-, impedimetric)

Prediction of infectious diseases

Telemetry, Daily health check, Healthcare, Telemedicine MEMS (respiration monitoring)

Collaborative research to overcome infectious diseases

Low-temperature plasma

Atmospheric pressure plasma jet
Plasma-treated solutions

Research
Nanotechnologies Semiconductor
devices

Nanoparticles Nitride-based LEDs
Antiviral surface coating

Plasma-on-Chip

Figure 2. Overview of this review. Highly collaborative research is required.

2. Technologies for sterilization of pathogenic viruses

2-1. Potential solutions

The mechanism for the sterilization of infectious viruses is known to have three principles: (i) disruption of virus structure and membranes, (ii) oxidative damage to virus contents involving enzymes, and (iii) genomic toxicity, i.e., destruction of DNA or RNA strands.

The novel coronavirus can be inactivated by a variety of chemical disinfectants, such as hypochlorite solution, alcohol, hydrogen peroxide, and glutaraldehyde. Key risks associated with the use of chemical disinfectants are supply shortages and shelf-life expiration.

Physical disinfection methods generate a biocidal compound *in situ*, and these methods often have a long lifetime and would thus have smaller associated supply risks. We review two examples of physical disinfection methods: (i) ultraviolet (UV) light and (ii) gas plasma technologies.

The inactivation of virus using UV light has attracted much attention over the last decade. Recent developments in virus inactivation using UV light are reviewed in section 2-2. The UV radiation spectrum can be categorized into wavelengths from 315 to 400 nm for UV-A, from 280 to 315 nm for UV-B, and from 100 to 280 nm for UV-C [4,5] (Fig. 3). UV light sources produce light by arc-discharge of Hg vapor and the formation of excited dimers in plasma discharge. The excited dimers are called excimers, for example, XeCl (308 nm), KrF (248 nm), KrCl (222 nm), ArF (193 nm), and Xe₂ (172 nm) [6]. Excimers spontaneously emit photons with transition from the excited state to the ground state. UV emission of the KrCl excimer with a wavelength of 222 nm is very promising as it is suitable for the disinfection of viruses on human skin

because UV-induced damage to the skin can be minimized by the limited penetration depth of this wavelength [7]. In addition, light-emitting diodes (LEDs) are an alternative and effective source of UV radiation to plasma-based lamps, and there are developments to extend their region of operation to shorter wavelengths in the UV-C range below 300 nm.

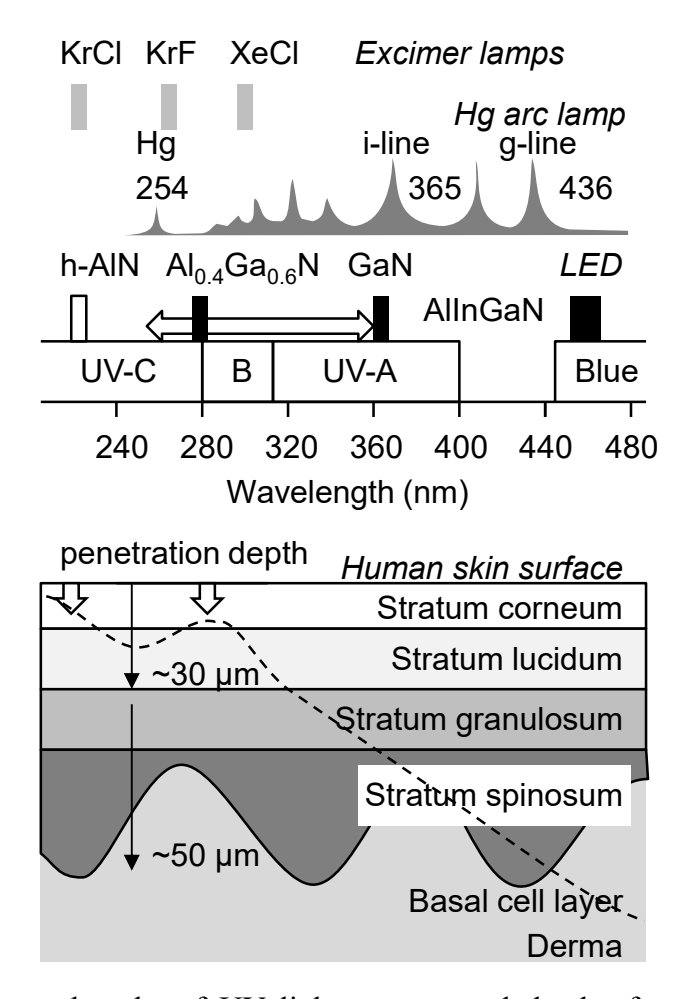


Figure 3. Radiation wavelengths of UV light sources and depth of penetration into human skin [7].

Recent developments in the inactivation of viruses by gaseous plasma are reviewed in section 2-3. Only a handful of papers on the plasma-based inactivation of viruses were reported by 2015. One of the earlier works that described the mechanisms

of plasma-based inactivation of viruses in solution by cold atmospheric pressure plasma was by Aboubakr *et al.* [8]. In 2020, Chen *et al.* demonstrated that argon cold atmospheric plasma irradiation could inactivate the SARS-CoV-2 virus on various surfaces including plastic, metal, cardboard, basketball composite leather, football leather, and baseball leather [9]. The potential role of gaseous plasma as an asset to healthcare during viral pandemics was reviewed by Bekeschus [10]. Bruggeman and Millar reported that plasma-induced singlet oxygen (O_2 $^1\Delta$) or peroxynitrous acid (ONOO) play key roles in the chemistry of virus inactivation, and other reactive oxygen and nitrogen species (RONS) can subject viruses to destructive oxidation, structural disintegration, and DNA damage, which demonstrate the usefulness of plasmas for virus inactivation and the effectiveness of reactive nitrogen species such as N_2O_5 [11].

Gaseous reactions in atmospheric pressure discharges were analyzed by various optical diagnostic methods, as reviewed by Takeda *et al.* [12]. Water dissociation generates H₂O₂ through hydroxyl radical (·OH) formation [13]. A plasma region in contact with a liquid surface has a very thin boundary layer between gas and liquid that provides a reactive field that is activated by bombardment with charged particles such as electrons and ions, and impingement of reactive neutral species such as ground state O atoms (O ³P), excited O atoms (O ¹D) and O₂ molecules (O₂ ¹Δg), O₃, and ·OH radicals. In air or a nitrogen-containing atmosphere, nitric oxide (·NO) plays a key role in the generation of nitrogen oxides such as HNO₂, HNO₃, N₂O, NO₂, N₂O₃, N₂O₄, and N₂O₅ [14]. In particular, for long-lived species in a liquid phase, the dissolution of these species generates NO₂ and NO₃ anions. HNO₂ is generated by reaction between ·OH and ·NO, and dissolution into liquid generates NO₂ and ONOO as reported by

Kurake *et al.* [15]. Therefore, an atmospheric pressure plasma source behaves as a source of RONS. This review covers recent developments in gas plasma technologies, in particular, RONS.

2-2. Ultraviolet light

2-2-1. 222 nm ultraviolet excimer lamp

The use of ultraviolet radiation C (UVR-C) lamps for inactivation of microbes, including virus, bacteria, and spores, has recently drawn significant attention due to the COVID-19 pandemic. UVR-C lamps are routinely utilized for surface sterilization. The application of conventional germicidal lamps that emit primarily 254 nm UVR to the human body is not approved for safety reasons, despite the usefulness of 254 nm germicidal lamps. The most critical effect of germicidal lamps on humans and experimental animals is skin cancer caused by genotoxicity. In that sense, the sterilizing potency and skin carcinogenic potency are two sides of the same coin. As an alternative, new devices that emit much shorter UV-C wavelengths than 254 nm UVR have emerged. Among them, 222 nm UVR has been reported to be harmless to the skin of mice in terms of the formation of cyclobutane pyrimidine dimers (CPD)s, although it has sterilizing ability comparable to that of 254 nm UVR [16]. There has been no clear evidence for safety with respect to acute and chronic exposure to skin in vivo. Therefore, more direct evidence of a lack of carcinogenicity of 222 nm UVR on human skin is required.

An animal model of xeroderma pigmentosum (XP) was used to investigate the acute and chronic biological effect of 222 nm UVR on the skin [17]. XP is known to be a genetic photosensitive disorder, and patients with XP have a severe and exaggerated response to UVR with a more than 10,000-fold increased risk of non-melanoma skin cancer and a more than 2,000-fold increased risk of melanoma before the age of 20 years, due to deficiency in repair of UVR-induced DNA lesions, including CPDs [18].

The UVR source used was a KrCl excimer lamp with an optical filter that

restricted emission from 200 to 280 nm wavelengths UVR. The installed filter was used to remove almost all but the 222 nm emission wavelength. Given that the energy between wavelengths of 200 and 230 nm is 100%, the energy for UVR wavelengths between 235 and 280 nm accounts for 0.13%. As for the component of the UV-B range, the energy between 280 and 320 nm accounts for 0.04% [19].

Acute cutaneous response after single-shot irradiation with narrow-band 222 nm UV was investigated. CPD formation in the epidermis was evaluated using hairless albino *Xpa*-KO (hereafter Xpa-KO) and hairless albino wild-type (wild-type) mice after 222 nm UVR irradiation. (*XPA* encodes the DNA repair protein, XPA, which is deficient in patients with XP-A.) Single-shot irradiation at 1.0 kJ/m² did not produce CPD in either genotype mice. The mice were then irradiated with 222 nm UVR at 5 kJ/m². Narita *et al.* reported previously that no CPD formation was observed in the dorsal skin of albino hairless mice by either a single-shot irradiation or ten days repetitive irradiation with 222 nm UVR at 4.5 kJ/m² [16]. 222 nm UVR at 5 kJ/m² produced CPD only in the uppermost corneal layer of both genotype mice, whereas strong CPD-positive cells were observed throughout the epidermal layer after either 254 nm UVR at 1 kJ/m² or broad-band (BB) UV-B exposure.

UVR-induced inflammation is considered to be a promoting factor for the development of skin cancer; therefore, the effect of 222 nm UVR irradiation was investigated with respect to inflammation in mouse skin. *Xpa*-KO mice are characterized by a highly photo-carcinogenic phenotype with a strong inflammatory response to UVR. This is a suitable model to predict human skin tumor formation. When the mice were irradiated with 222 nm UVR at 10 kJ/m², which was estimated to be 100 times a sterilizing dose, erythema were not observed in either genotype mice,

while strong erythema was observed in *Xpa*-KO mice after exposure to either 254 nm UVR or BB-UVB.

To investigate the chronic effect of 222 nm UVR, a protocol in which 100% of *Xpa*-KO mice would develop skin tumors after 10 weeks irradiation with BB-UVB was adopted. Based on an estimated sterilizing dose of 222 nm UVR at 0.1 kJ/m² and a 10,000-fold greater susceptibility to develop UVR-induced skin tumors in patients with XP in comparison with the general population, the dose of 222 nm-UVR per exposure was set for wild-type at 5.0 kJ/m² and that for *Xpa*-KO mice at 0.5 and 1.0 kJ/m². Dorsal skin was irradiated with 222 nm UVR twice a week for *Xpa*-KO mice, and three times a week for wild-type mice. In contrast with the previous study that showed a 100% incidence of skin tumors in *Xpa*-KO mice by exposure to BB-UVB [19], no tumors were observed in any of the mice after irradiation with 222 nm UVR, which indicates that 222 nm UVR did not exert photo-carcinogenic effects.

222 nm UVR is effective for disinfection because it produces CPD in microbes on a surface [20], and it is safe for animals because the 222 nm UVR wavelength is too short to penetrate the stratum corneum to reach the nuclei of the basal cell layer of the skin, where cancer stem cells are considered to reside. There are additional publications with respect to the effects of 222 nm UVR on biological bodies [21-28]. It can be concluded that 222 nm UVR lamps are safe for the sterilization of human skin, with no evidence of skin carcinogenesis after long-term exposure, even for mice with high skin photo-carcinogenic susceptibility, in addition to no inflammatory reactions or harmful effects on mice skin.

2-2-2. AlGaN-based deep UV LEDs

AlGaN is one of the semiconductor ternary alloys with the largest bandgap energies ($E_{\rm g}$: 3.4–6.0 eV) that emits and absorbs electromagnetic radiation at wavelengths from 200 to 360 nm. This ternary alloy is a part of the nitride semiconductor family, AlGaInN. It should be noted that another ternary alloy of the nitride semiconductors, GaInN, has been used in high-efficiency blue LEDs that emit at wavelengths from 450 to 470 nm. The 2014 Nobel Prize in Physics was awarded for the invention of such high-efficiency blue LEDs.

Under the influence of the global coronavirus outbreak, AlGaN-based deep ultraviolet (DUV) LEDs that emit at wavelengths from 260 to 280 nm have attracted significant attention as next-generation light sources toward water purification and air sterilization [29]. DUV LEDs have features such as being Hg-free, and having a small footprint, immediate turn-on characteristics, and direct current operation with a couple of voltages, which are important benefits for the manufacture of small compact purification/sterilization modules that could be attached to air conditioners and water taps, as examples. However, DUV LEDs currently suffer from a very low power conversion efficiency (ca. 4%) and short device lifetimes (ca. 10,000 h). It is interesting that the DUV LEDs show significantly inferior characteristics compared to blue LEDs, which exhibit very high efficiency (ca. 80%) and long lifetimes (ca. 40,000 h) [30], even though they are made from the same nitride semiconductor family material.

Figures 4(a) and (b) show schematic diagrams of a GaInN blue LED and an AlGaN DUV LED, respectively. The bandgap of the active region emitting light in the $(Al_{0.4}Ga_{0.6}N)$ DUV LED is an E_g of ca. 4.4 eV, which is much larger than that in the blue LED, GaInN (E_g of ca. 2.7 eV). Consequently, the surrounding p-type and n-type

layers must have larger bandgaps in the DUV LEDs than in the blue LEDs. For instance, GaN ($E_{\rm g}$ of 3.4 eV) pn layers are sufficient in the blue LEDs, in which a hole concentration of ca. 1×10^{18} cm⁻³ is available. In contrast, Al_{0.6}Ga_{0.4}N ($E_{\rm g}$ of 5.0 eV) p-type and n-type (pn) layers are required in the DUV LEDs, but have a hole concentration that is two orders of magnitude less. In other words, such p-type wide bandgap materials are very close to insulating materials, such as SiO₂. Thus, absorptive p-GaN layers have been reluctantly used in current DUV LEDs for hole injection; however, those results in high light absorption in the p-GaN layers.

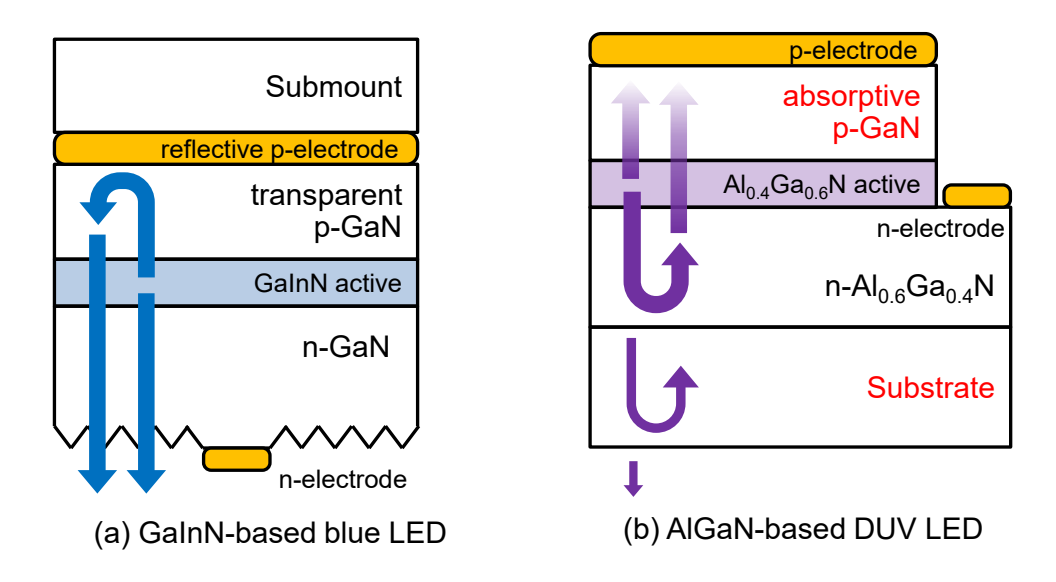


Figure 4. Schematic diagrams of (a) a GaInN-based blue LED and (b) an AlGaN-based DUV LED. While light extraction engineering has been fully adopted in the blue LED, further development is required in the DUV LED.

Three things are required to achieve high-efficiency DUV LEDs. One is a high hole concentration and/or an alternative hole injection scheme in the wide bandgap AlGaN. Polarization p-type doping [31] and/or tunnel junctions [32] have been investigated as solutions. The second requirement is light extraction engineering for DUV LEDs, including substrate removal for higher light extraction from the backside.

Such light extraction engineering has been demonstrated in blue LEDs [33]; however, feasible solutions are still required for DUV LEDs. The last requirement is long device lifetime. Device degradation mechanisms under operation must be understood to provide positive feedback to material growth, device processing, and packaging. Nevertheless, DUV LEDs are expected to become a next-generation energy-saving UV light source for the simultaneous accomplishment of a safe environment and low carbon emissions.

In the case study of DUV LED sterilization, Liu *et al.* reported the growth of high-quality AlN templates with threading dislocation densities as low as 6×10^8 cm⁻², which led to 275 nm DUV LEDs with a light output power of 10 mW at a current of 100 mA (corresponding to an external quantum efficiency of 2.65%). An array of 15×13 DUV LED chips was then integrated into a sterilization light source at a size of 3.0×3.6 cm², with a light output power as high as 2 W at a current of 1.3 A. They also reported that a one-second exposure time from the light source at 94 mW/cm² is sufficient for the complete elimination of SARS-CoV-2 [34].

Toyoda Gosei Co., Ltd, an LED manufacturer, has also announced that DUV LEDs are highly effective to inactivate the SARS-CoV-2 virus [35]. They used their DUV LED products (276 nm wavelength, 55 mW power output, 350 mA current injection) to irradiate the SARS-CoV-2 virus at 2.6 mW/cm², whereby more than 99.999% of the viruses were inactivated in 5 s [35].

History shows that the replacement of vacuum tube devices with solid-state devices is desirable. Therefore, further progress in the development of DUV LEDs is expected.

2-3. Low temperature plasma technologies

2-3-1. Sterilization by plasma I

Plasmas for the decontamination of airborne viruses and viruses on surfaces have been investigated [36], as described elsewhere [11]. While the work was often motivated by airborne and food-borne animal viruses, the potential of plasma technology in the current combat against the COVID-19 pandemic is emerging.

A significant focus of the initial research at the University of Minnesota was on the mechanisms that underpin plasma-based inactivation of viruses. Earlier work on plasma-enabled virus inactivation was performed with atmospheric pressure plasma jets in different gases to enable the selective tuning of virus inactivation and to determine the key reactive species that enable virus inactivation [37,38]. It was shown that both reactive oxygen species (ROS) and reactive nitrogen species (RNS) can play a significant role in virus inactivation. Detailed studies on the feline calicivirus using an oxygen plasma, including scavenger studies, showed that singlet oxygen (O_2 ($^1\Delta_g$)) plays a key role in virus inactivation [39]. This result has been complemented with studies using molecular beam mass spectrometry, liquid phase analysis, and proteomics that have enabled the tracking of O_2 ($^1\Delta_g$) from the plasma source to its oxidative effect on the virus capsid of feline calicivirus [39,40].

RNS have also been identified as key for the inactivation of viruses with air-based plasma sources [41]. In addition, detailed control studies of the key reactive species have shown a strong correlation between NO₂ and virus inactivation [42]. Detailed control experiments showed that mixtures of O₃ and NO₂ that produce N₂O₅ resulted in significant viral inactivation. This was supported by the independent work by the Kaneko group described in the next section. It is likely that the dominance of N₂O₅,

which is a stable species, is related to transport limitations or specific reactions in the liquid phase.

In addition to the inactivation of virus suspensions, virus inactivation by gas-phase plasmas on substrates was also considered. Direct contact between plasma and a substrate was shown to lead to much more effective inactivation of viruses compared to remote plasma treatment for which long-lived RONS in the plasma effluent enable inactivation. Nonetheless, direct plasma-substrate interactions are highly substrate-dependent and have limitations with respect to the morphology and composition of the substrate. This limitation has motivated our focus on indirect plasma treatment. A key requirement for effective virus inactivation by plasma effluents is the need for surface humidity [41].

While the plasma inactivation research at the University of Minnesota used feline calicivirus in many studies, they extended the work on food substrates and also reported effective inactivation of human norovirus and Salmonella Heidelberg [43,44]. Detailed optimization studies show that it is possible to achieve similar energy efficiencies for plasma inactivation as for UV-based inactivation [45]. A key advantage of plasma is the lack of shadowing effects that are present with UV, which opens the path for plasma-based decontamination of complex 3D objects.

In addition to the disinfection of substrates and solutions, and motivated by the airborne transmission of some viruses, they also investigated the inactivation of an aerosolized virus by a dielectric barrier discharge in a model wind tunnel [46]. The study was originally motivated by virus transmission in animals and the porcine reproductive and respiratory syndrome (PRRS) virus was used for the tests. The dielectric barrier discharge source used could achieve a 3 log reduction in viable virus

titer with a plasma-aerosol contact time of only 15 ms, the time scale of which is compatible to the residence time of air in heating, ventilation, and air-conditioning (HVAC) systems. It is important to note that any viable virus remaining in the treated airflow was below the detection limit. The plasma technology could have similar effectiveness to minimum efficiency reporting value (MERV) filters or electrostatic precipitators and does have a key distinctive feature: analysis of the virus genome showed that the inactivated virus was not removed from the air stream, although the plasma did inactivate the virus and it is no longer infectious.

In view of the growing data that support SARS-CoV-2 being mainly transmitted through aerosols, the potential of plasma-based airborne inactivation, although only tested on animal viruses, shows promise for plasma technology to contribute to combating the major societal challenges of the COVID-19 pandemic.

2-3-2. Sterilization by plasma II

Controlled synthesis of short-lived reactive species using gas-liquid interfacial plasmas for sterilization and virus inactivation is reviewed here. Atmospheric-pressure plasmas in contact with a liquid, which are defined as gas-liquid interfacial plasmas, are widely used in the medical, agricultural, and public health fields. Various stimuli, such as electrical, chemical, mechanical, and thermal stimuli, are generated in gas-liquid interfacial plasmas and delivered to microorganisms, biological cells, and tissues. Among these stimuli, RONS as chemical stimuli are particularly important for sterilization and virus inactivation toward public health. The Kaneko group has experimentally investigated the generation and reaction of RONS [47], especially short-lived reactive species, using several lab-built gas-liquid interfacial plasma devices, and has demonstrated sterilization and virus inactivation.

They have developed a humidified air plasma effluent gas device [48], whereby the supply of liquid water into atmospheric pressure air discharge plasma humidifies the effluent gas and significantly improves the sterilization and virus inactivation effects, i.e., suppressing conidium germination of plant pathogenic fungi [48,49] and inactivation of the tobacco mosaic virus in a liquid droplet [50]. The roles of water supply to the air plasma can be deduced as hydrogen atom supply and cooling of the plasma effluent gas to increase hydrogen-containing precursors for the generation of antibacterial species, i.e., HNO_{2 (aq)} and H₂O_{2 (aq)}. Gas cooling by the latent heat maintains a low density of ozone (O₃) in the plasma effluent gas, which can activate dinitrogen pentoxide (N₂O₅) chemistry in the gas phase and at the gas liquid interface [47].

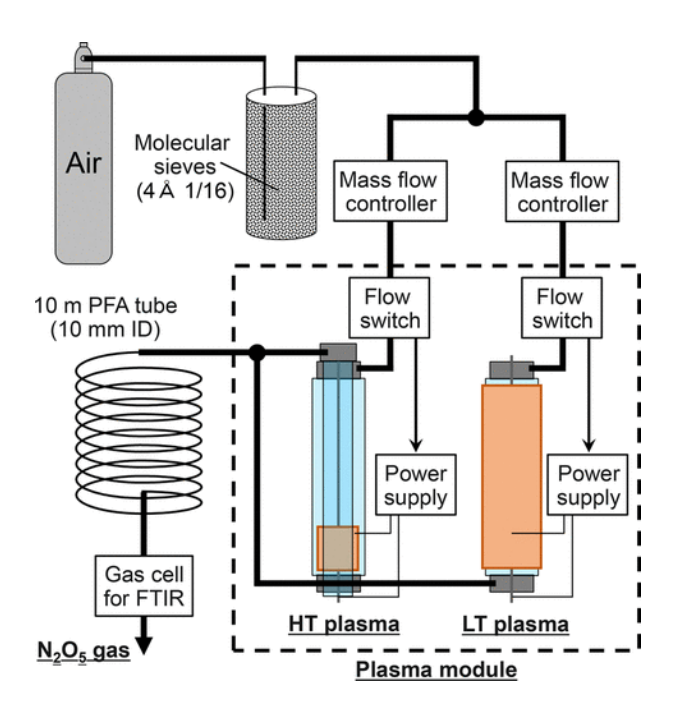


Figure 5. Experimental schematic diagram of the plasma system for electric N₂O₅ production from air. (Reprinted with permission from Ind. Eng. Chem. Res. 60, 798 (2020). Copyright (2020) American Chemical Society.)

 N_2O_5 chemistry has attracted attention in a wide range of academic fields, but has yet to become widespread because typical synthesis methods for high-purity N_2O_5 require multiple hazardous raw materials (that require handling with much care). However, a newly developed plasma device, shown in Figure 5, has achieved a high density of N_2O_5 (up to 200 ppm) with high selectivity, produced exclusively from air with power consumption below 100 W [51], which is expected to promote the application of N_2O_5 chemistry.

An experiment on bacteriophage Q beta (Q β phage) inactivation was conducted with air plasma effluent gas, of which the RONS composition can be N₂O₅ rich. Q β phage is a positive-strand RNA virus which infects bacteria, and could be used in the antiviral test in the Japanese industrial standards (JIS) or the international organization for standardization (ISO) standard. A Q β phage suspension at 10⁸ plaque-forming units

(PFU) is typically atomized into 5 μ m by a nebulizer. The phage-contaminated mist is transported via room air flow convection into a coaxial flow reactor to mix with the air plasma effluent gas. The mist is collected into a bottle with phosphate buffer solution for up to 900 s, controlled by the flow valves. The residence time of the virus mist in the reactor is less than 3 s, estimated from the plasma effluent gas flow rate of 2 standard liters per minutes (slm) and the volume of the flow reactor. With a N_2O_5 dominant plasma effluent gas, the PFU is below the detection limit, which indicates that N_2O_5 can be a key species to inactivate the Q β phages. From these results, the specific gaseous species, such as N_2O_5 , can be expected to be effective in inactivating coronavirus.

Kaneko *et al.* have also developed an air plasma exposed solution (PES) spray device for plant pathogen control. Direct contact with the plasma in the PES spray device is expected to yield a high concentration of short-lived reactive species that are then transported to the target objects within a short time. PES spray for 5 s significantly suppressed germination of a fungal conidium of a strawberry pathogen. In addition, the germination suppression efficacy is not monotonically modulated by the gas and solution flow rates for PES generation. This sterilization effect was not reproduced by the combined addition of long-lived reactive species (H₂O₂, NO₂⁻, NO₃⁻) in the liquid phase. It is suggested that several short-lived reactive species that are generated with control of the solution flow rate and contribute to germination suppression (sterilization).

An air plasma-effluent-gas dissolved solution (PEGDS) spray device has been developed [52]. The PEGDS spray device relies on dissolution of the plasma effluent gas into distilled water for practical use in the public health and agricultural fields. The performance of the PEGDS device is characterized by the suppression of conidial

germination of plant pathogens, and the reactive species are generated in both the gas and liquid phases. The results suggest that O₃ could be responsible for the germination suppression effect under the given operating conditions, of which the lifetime is shortened by co-dissolved reactive species. This suggests that an O₃-dependent anti-bacterial effect can be tuned by the co-dissolved reactive species, which could balance the anti-bacterial effect, the environmental release of the generated species, and plant responses.

2-3-3. Sterilization by plasma III

Non-thermal atmospheric pressure biocompatible plasma (NBP) sources and their characteristics when operated at atmospheric pressure have been investigated for inactivation of coronaviruses [53-56]. In this section, sterilization by plasma is reviewed in terms of plasma-generated RONS.

Figure 6(A) shows a schematic illustration of a nonthermal atmospheric pressure plasma jet. Air or nitrogen gases are used for plasma generation. Typical time-dependent voltage and current curves of the plasma jet are shown in Fig. 6(B), where the discharge power was less than 2 W in this experiment. Figure 6(C) shows a typical optical emission spectrum (OES), which indicates the associated RONS are ·NO, ·OH, excited N₂ molecules, and atomic oxygen atoms. The plasma density was characterized to be ca. 8×10^{15} cm⁻³ by simple Michelson interferometry without a heterodyne modulator. The electron temperature was characterized to be ca. 1.7 eV using the stepwise ionization model with an ambipolar diffusion process [54].

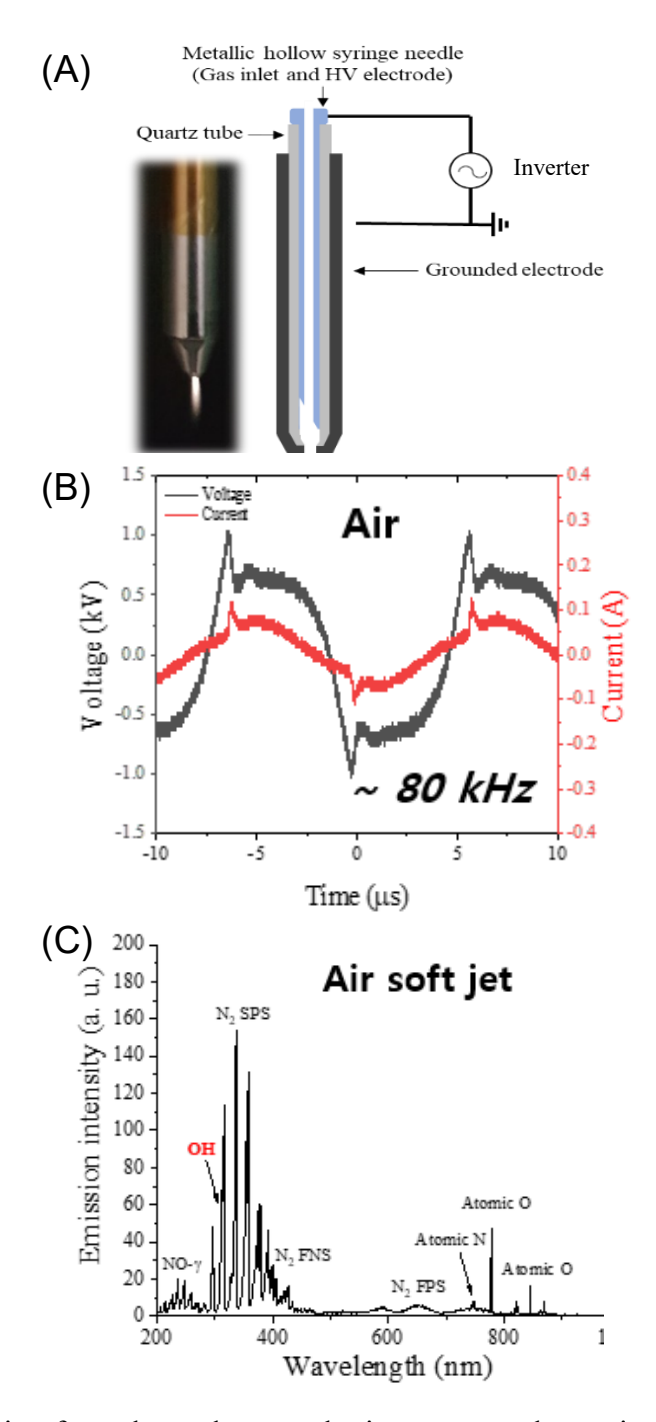


Figure 6. Schematic of nonthermal atmospheric pressure plasma jet called air NBP jet (A), and time-dependent current-voltage (B), and optical emission spectrum (OES) (C).

The results shown in Fig. 7 indicated that the plasma electron density $n_{\rm e}$ (red dots) had a strong correlation with the plasma dissipated energy (black squares) for the

transient plasma jet in a cycle as the breakdown voltage increased. Under the conditions of a dissipated energy of 0.3 mJ, which was generated by an electric field of ca. 23 kV/cm, and n_e of ca. 8.0×10^{15} cm⁻³, RONS such as ·OH, H₂O₂, ·NO, and NO₂ were produced in the plasma and used in the following experiments.

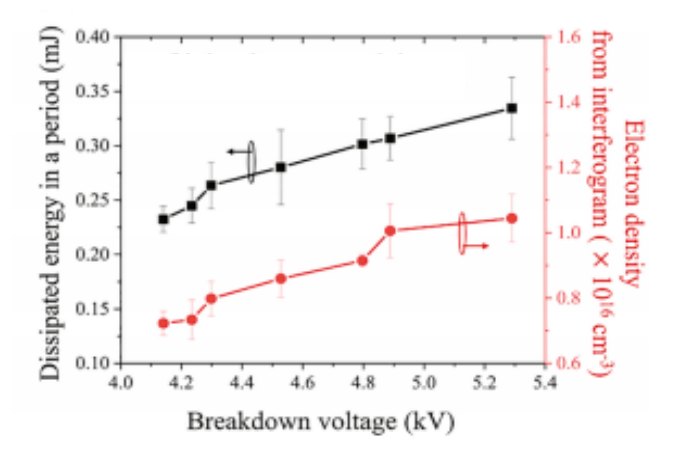


Figure 7. Plasma dissipated energy in a period (black squares) and electron density (red dots) as a function of breakdown voltage. The plasma electron density was obtained using Michelson interferometry for a transient plasma jet [54].

Figure 8 shows the typical NO_2 and NO radical densities as a function of the pulse duty ratio in a plasma jet obtained by cavity enhanced absorption spectroscopy [58]. The average NO_2 density in an air plasma jet was ca. 3.0×10^{16} cm⁻³. The plasma jet was operated with a change in the pulse duty ratio from 10% to 55%. The NO_2 density ranged from around 2.0×10^{15} cm⁻³ to 5.2×10^{16} cm⁻³. The average NO density ranged from 4.0×10^{15} cm⁻³ to 8.2×10^{15} cm⁻³. Overall, the NO density was shown to be 10 times smaller than that of NO_2 .

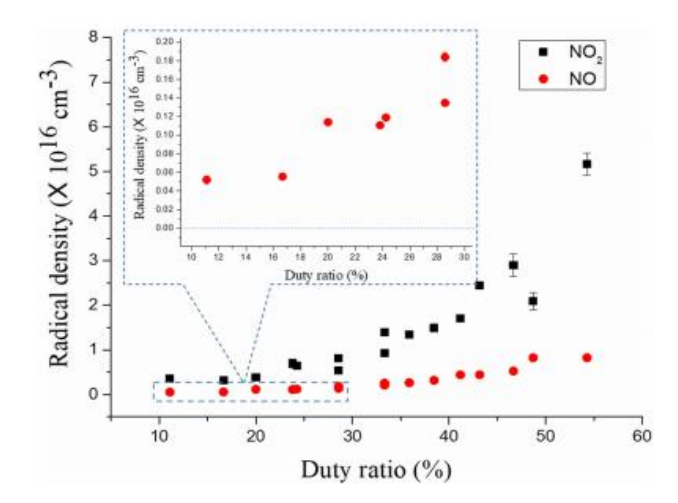


Figure 8. Typical NO₂ and NO radical densities as a function of the pulse duty ratio in a plasma jet [57].

RONS generated by the NBP jet were investigated for inactivation of the human coronavirus 229E. The 229E coronavirus was isolated and purified after appearance of an approximately 80% cytopathic effect (CPE) in MRC5 (human fibroblast lung cell line) culture using DMEM (Dulbecco's Modified Eagle Medium) with 2% fetal bovine serum. Inactivation of 229E was evaluated from the TCID₅₀. Figure 9 shows log(TCID₅₀/mL) for human coronavirus 229E with various air NBP jet exposure times, ranging from 30 s to 300 s with a control condition (0 s). TCID₅₀ decreased with an increase in the NBP jet exposure time. After a plasma treatment time of 300 s, TCID₅₀ titers achieved a 98% decrease in viable viral particles [58]. Choi's group also showed the RONS had effects for cancer treatment.

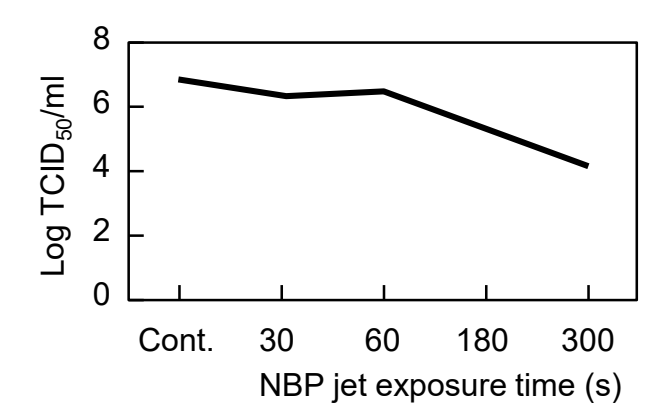


Figure 9. Decline in TCID₅₀/mL (median titer) of coronavirus 229E as a function of the air NBP jet exposure time.

The electron temperature, plasma density, and RONS were characterized for oral administration of plasma-treated water (PTW) to treat non-small cell lung cancer, as well as human coronavirus inactivation by NBP based on synergistic plasma UV photolysis and a diffusive molecular transport mechanism. The physical and chemical combination of the plasma-based techniques played key roles for the sterilization of pathogens and viruses.

3. Technologies for virus sensing/prevention of infection

Transportation developments have connected the global community so that people can conveniently visit various areas within a short time. However, the development of the transportation has increased the possibility of virus spreading. Virus-infected people should be stopped by quarantine at airports, but how can such infected people be detected? In the standard quarantine process, self-assessment and thermography play important roles. When a passenger is suspected of being infected, infection must be evaluated. Therefore, rapid detection methods with high sensitivity must be developed. For this purpose, we will review recent developments in the methods for the sensing of viral pathogens and the prevention of infectious disease (Fig. 10).

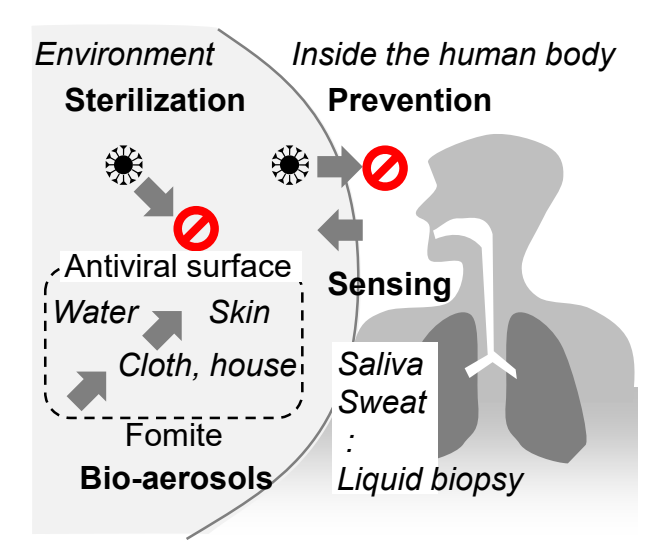


Figure 10. Technological targets for the prevention of viral infection. Airborne viruses are transmitted to a susceptible host in the form of aerosols that are generated by expiration evaporation and by contact with infected or deposited surfaces and fomites. To obtain environmental information with respect to infectious viruses is also important to prevent the infection; therefore, virus sensing methods should be developed.

3-1. Viral filtration with membrane filters

Viruses are small in size, from 20 nm to a few hundred nanometers. Such a small size means it is difficult to separate viruses solely using the size exclusion principle. Membrane filtration technologies are implemented (Fig. 11); commercially, filtration sizes are categorized into microfiltration (0.1 to 10 μ m), ultrafiltration (0.01 to 0.1 μ m), nanofiltration (<10 nm), and reverse osmosis (10 nm for amino acids, sugars, and salts) [59].

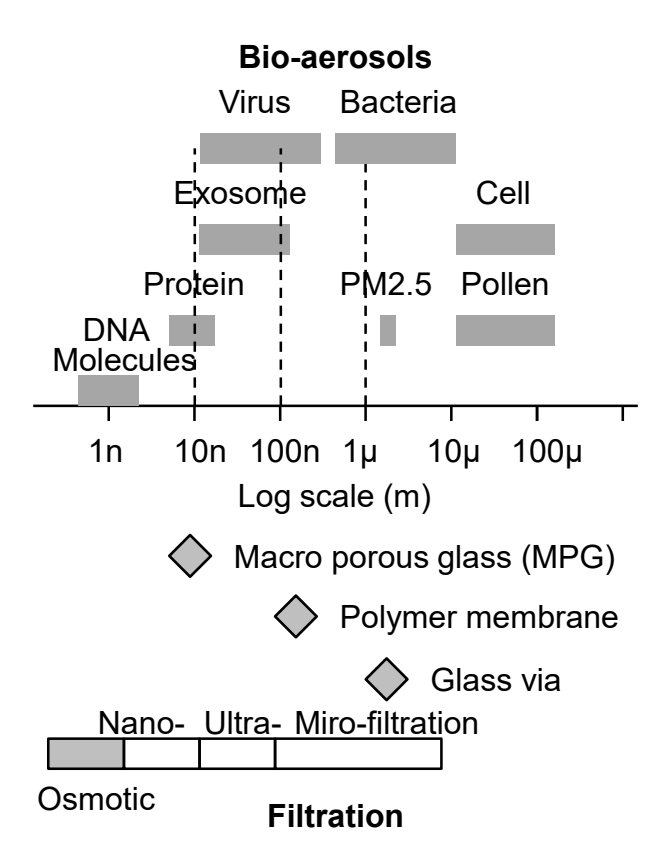


Figure 11. Size of the sensing targets for bio-aerosols involving viral and bacterial pathogens, and cells. The filtration category and corresponding filtration device are indicated. Bio-aerosols are generated in human exhalation, splashed saliva, sweat, etc.

During filtration, high pressure applied to one side of the membrane squeezes the cells, while the lower pressure on the opposite side draws the cells to it [60]. There

are three solutions to solve this cell-squeezing problem: (i) micro- and macroporous structures, (ii) top-down fabrication of size-unified filtrate holes, and (iii) microfluidic control with surface functionalization of hole-interiors and structural shapes.

First, ceramic membranes formed by spinodal decomposition are suitable for ultrafiltration. A size-controlled macroporous glass (MPG) membrane was synthesized by control of the micropore size from 10 to 1200 nm by changing the heating temperature and time based on the spinodal decomposition of B₂O₃, Na₂O, and SiO₂ in phase separation [61]. This filter was demonstrated to separate extracellular vesicles with sizes of 50–500 nm in diameter.

Second, in accordance with the size exclusion principle, the variation of filtrate hole sizes is indispensable to achieve filtration properties. Therefore, polymeric membrane filters with precise, dense, and unified holes are fabricated by photolithographic techniques and plasma etching methods [62]. A key point in the fabrication of polymeric membrane filters is the handling method of the membrane during manufacture [63]. For example, with ethylene tetrafluoroethylene (ETFE) membranes, 380,000 top-down-fabricated highly packed through-holes were demonstrated to collect circulating tumor cells in human blood samples [64]. This type of filtration is suitable for separation based on the size exclusion principle.

Third, the hydrophilicity and hydrophobicity of the surface of hole interiors in filter membranes affect the flow speed of liquids through the membrane [65]. Control of the surface tension of these interiors enables liquid transport flow to be driven by internal Laplace pressure difference based on the surface tension of droplets placed on the front and back sides of the tested substrates. Furthermore, tapered shape holes similar to a micro sand timer in a glass membrane device can allow liquid flow by a

similar Laplace pressure difference [66]. These effects in filtration processing have a considerable effect on performance. Membrane filtration can thus provide an effective way to remove pathogenic viruses from liquids and air for the prevention of virus infection.

Diagnostics are required with minimal burden on patients. Small amounts of bodily fluids are collected from blood or urine for a liquid biopsy [67], where biomarkers are captured and genetic information can be analyzed. However, this involves invasive diagnostic methods, whereas bio-aerosols that are collected from exhalation, saliva, and sweat could instead be collected for analysis. Such diagnostics could lead to the realization of simple daily health checks. Combined with big-data information technology, unobtrusive medical and health monitoring could become possible.

3-2. Antibacterial and antiviral coating of copper etc.

Copper alloys are known to be effective antimicrobial surfaces against a range of bacteria and fungi. Warnes and Keevil reported that norovirus is inactivated at room temperature on dry copper alloy surfaces containing over 60% copper [68]. They also reported that the rate of inactivation was initially very rapid and proportional to the copper content of alloys tested. Cu(I) was identified as the primary effector in the copper surface inactivation of norovirus, whereas Cu(II) is not effective for the inactivation of norovirus. Fujimori *et al.* reported that nanosized copper(I) iodide particles with an average size of 160 nm have antiviral characteristics to inactivate influenza viruses, potentially by ·OH generation [69]. In addition, they reported ·OH radical generation only for Cu(I) samples [70]. A humidified surface contains water and metal oxidation catalyzes the redox reaction, given by Cu + O \rightarrow Cu₂^(I)O + e $^-$ or Cu₂^(I)O \rightarrow Cu^(II)O + e $^-$ and H₂O + e $^ \rightarrow$ H· + ·OH. Zerbib *et al.* researched the efficacy of copper as an antimicrobial agent in a long-term nursing home facility, and concluded that the risk of hand-transmitted health care-associated infection was significantly lowered in areas equipped with copper surfaces [71].

Against COVID-19, Doremalen *et al.* reported as a rapid correspondence in April 2020 that SARS-CoV-2 is less stable on copper than on plastic or stainless steel, and viable SARS-CoV-2 virus was reduced to the detection limit within 10 hours of application to these surfaces [72]. Cold spray coating is a method of deposition onto a surface through bombardment of particles at lower temperatures than their melting point by injection of source materials in powder form into a thermal plasma. Unlike thermal spray deposition, the deposition particles can be transported to a surface by flow within an ultrasonic gas at low temperature, which can prevent thermal damage to the substrate.

Hutasoit *et al.* attempted to coat copper onto touch plates by employing a cold-spray coating technique and identified that 99.2% of SARS-CoV-2 was inactivated after 5 h of exposure to the as-deposited copper coating [73]. This report also noted that the copper coating on in-use stainless steel push plates was completed in 7 min and the copper-coated plates could be redeployed into service within 17 min [73]. Such a quick and easy fix approach is practically important to mitigate the spread of the COVID-19 virus.

Evaluation of the antimicrobial activity of 906 metal-containing compounds led Frei *et al.* to highlight highly antimicrobial metals [74]. Despite the mechanism for the antimicrobial activity being unclear, metal complexes act uniquely to exchange or release ligands, generate ROS, and promote the redox activation and catalytic generation of toxic species or deplete essential substrates [74]. In addition to copper, the antiviral activity of composites of silver nanoparticles and chitosan against H1N1 influenza A virus was reported by Mori *et al.* [75]. Naked silver nanoparticles with diameters from 2 to 15 nm exhibited cytotoxicity from 20 ppm onwards, as reported by Jeremiah *et al.* [76]. The antiviral activity of silver nanoparticles was also enhanced by irradiation of UV light at a wavelength of 365 nm (UV-A) because large amounts of hydroxyl radicals are generated, as reported by Nakamura *et al.* [77]. The essential mechanism of antiviral activity is thus considered to be the generation of reactive species that kill bacteria and inactivate viruses on the surfaces.

Clothing is produced from fabrics, textile, and fibers, both natural and synthetic, such as cotton, silk, wool, leather, nylon, and polyester [78]. Textiles are used for outdoor garments as protection against moisture, wind, and cold, combined with good perspiration transport to the outside. Natural or artificial textiles are fragile under

processes at temperatures higher than 100 °C. However, Ti-O coating is possible in a roll-to-roll process at low temperature using high power impulse magnetron sputtering (HiPIMS) technology [79,80].

Titanium oxide thin film under irradiation with visible light acts as a photocatalyst for the decomposition of H₂O and evolution of pure H₂ and O₂ [81,82]. This mechanism for this photocatalytic reaction is explained as a photo-generated electron in the conduction band reduces the oxidized state of metal oxides and photo-generated holes in the valence band oxidize adsorbates on the metal oxide surface [83]. At present, photocatalysts such as Ti-O, TiO₂, and nitrogen-doped TiO₂, and the antiviral activity of visible-light-sensitive Cu(II) and Fe(III) nanocluster-grafted TiO₂ have been reported by Miyaguchi *et al.* [84,85] and Kajita and colleagues [86,87]. There have also been reports of the plasma-assisted coating of photocatalytic films on surfaces [88-90]. In terms of other metal oxides, the photocatalytic activity of nanostructured tungsten oxides was reported by Feng *et al.* [91]. There have also been reports of silver-doped ZnO [92], ZnS and ZnO films [93], and Fe₂O₃ nanotubes and Cu₂O [94]. Such research has meant that antiviral coating on textiles is available at present.

Wool fibers and wool fabrics are superior natural textile materials; however, nanosized silver particle coating of wool has not been realized, because of the cuticle structure of the outer surfaces of wool fibers. Complex forms of silica and silver particle mixtures have been reported to provide good adhesion properties of the silver nanoparticles on wool fabrics [95].

Plasma coating technologies have enabled the coating temperature to be lowered so that various surfaces can be coated with copper (Fig. 12).

Antifouling, Antiviral, Antimicrobial

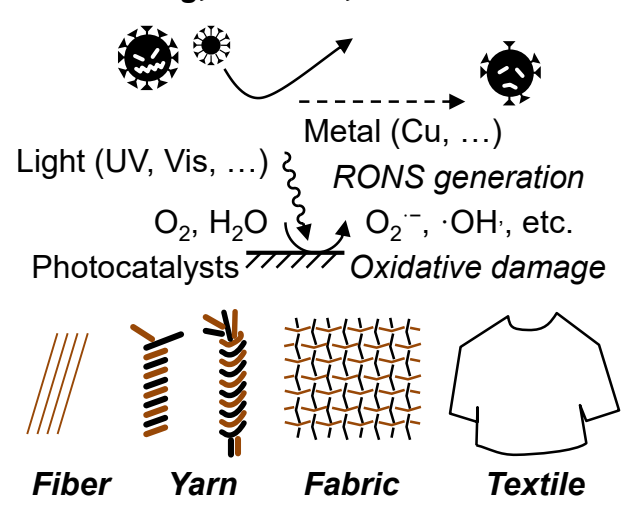


Figure 12. Antifouling, antiviral, and antimicrobial coating technologies that utilize plasma processing have enabled the coating of nanotechnology-based functional materials at low temperatures.

4. Technologies for the prediction of infection

One promising technology towards the control and ending of infection could be the prediction of infection. If we can predict infection of a person before being infected, then the person could be isolated to control the infection. However, to determine a person being infected is not an easy task. Small changes under typical physical conditions must be detected. Technologies for the sensing of viruses as discussed in the previous section should be improved further in terms of detection limits and ease of operation protocols (Fig. 13).

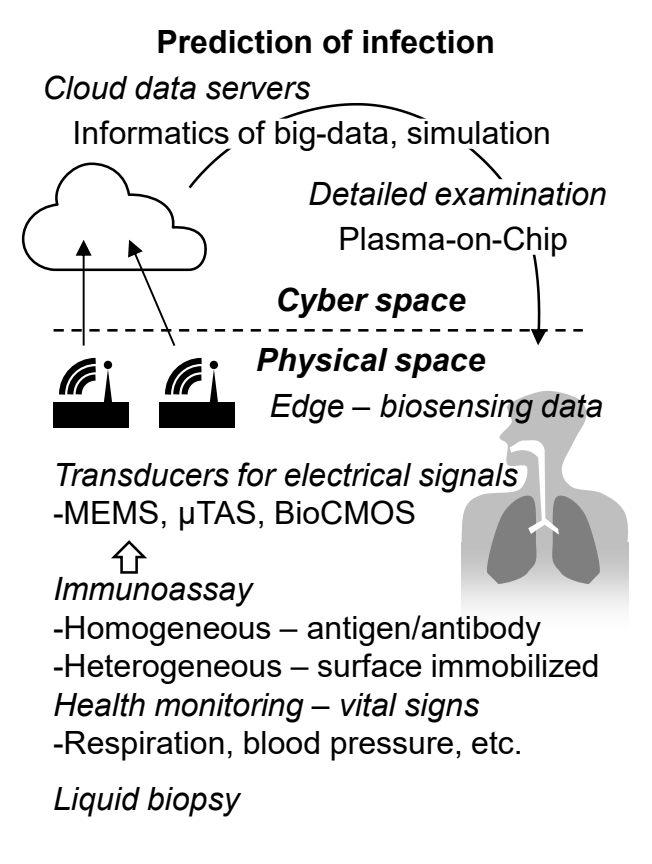


Figure 13. Health diagnostics is a key technology for the prediction of infection before infection spreads. Advances in information-communication-technology (ICT) enable the analysis of social trends of health based on the big data of biosensing signals that are transduced in electronics using microelectromechanical systems (MEMS) and BioCMOS technologies.

Virus detection using nanotechnologies were categorized by Chintagunta *et al.* [96] into diagnosis, treatment, and prevention of COVID-19. These involve technologies such as nanoparticle-assisted diagnostics, antibody assays, micro total analysis system (μ-TAS) flow immunoassay, and nanomaterial biosensors. Potential applications of nanotechnologies have also been discussed by Zare *et al.* [97]. They reviewed and reported challenges in device development for the detection, prevention, and treatment with respect to biofilm formation, and implant associated infection [97]. In μ-TAS fabrication, the plasma processes used for microfluidic devices involve surface activation, grafting, polymer coating, etching, and crosslinking, which are becoming key technologies [98]. Anti-biofouling technologies based on plasma processing are being widely developed [98].

Remote diagnosis is also an effective approach because it avoids a possibly infected person having to enter a medical institution. Besides, further important technology can be prediction of infection. Analysis of the big data of physical conditions can be used to predict if a person is infected.

In the future, as sensor networks mature and information technology is further developed, we will be able to predict trends in society. Prediction has the same problem as the dynamical control of machine systems. Biological cells are widely considered to be non-equilibrium dynamical systems. The internal state of a cell is regulated by sensory states obtained by sensing the surrounding environment. This mechanism is called homeostasis. Modeling of the homeostatic dynamics has not yet been achieved completely; however, Bayesian inference is a method that can statistically solve such complex problems. In the field of measurement and control, i.e., system identification, having a large number of the sensor signals promotes a data-driven scientific approach.

In system engineering, the internal state continues to change by action and senses again the change in the variables. The system can then be controlled by sense and action. To consider more fundamental principles in regard to this sense and action, free energy minimization is essential [99]. If a system is defined to have a set of possible internal states, then the internal state is determined by minimization of the free energy, i.e., the sum of enthalpy and entropy. Therefore, information for unknown variables (states) are obtained to reduce the free energy and increase the (Shannon) entropy. In other words, complexity and accuracy are reciprocal, as in the contrary theorem. In the development phase, evaluation of hypothetical prediction must be carried out.

To evaluate hypotheses obtained in the informatics in the cyber space should be done with the 3R principle. In terms of ethical issues, there are many hurdles to overcome before clinical tests. Even the animal tests for preclinical tests have the 3R principle: replacement of animal experiments with alternative methods, reduction of the number of animals used, and the refinement of animal experiments that emphasize minimal pain and distress for the animals [100]. Besides the 3R principle, attention must be paid to species-specific differences between the animal subject and humans. Therefore, the use of human-derived cells has become a standard method for the analysis of virus behavior in living bodies. For this purpose, we will review the *Plasma-on-Chip* technology later.

4-1. Sensing of coronavirus with nanomaterials

Nanoparticle-based electrochemical, optical, mass-sensitive, colorimetric, and immunoassays have been conducted. This section focuses on the detection of electrical conductance changes after the binding of antigens to immobilized antibodies on nanomaterials.

Huang al.demonstrated the graphene-based biosensors with et functionalization of the anti-E. coli O and K antibodies (i-DNA Biotechnology) using 1-pyrenebutanoic acid succinimidyl ester as a linker [101]. They could detect E. coli binding by the change in the electrical conductance of a graphene transistor [101]. Kim et al. reported that a graphene-based device could be used to detect the molecular absorption of botulinum neurotoxin that consists of approximately 150k base-pair (bp) proteins [102]. With the immobilization of linkers of antibody-antigen binding sites on the graphene transistor, the electrical conductance of the transistor was modified by the adsorption of antibody proteins [102]. Narayanan et al. reported that graphene and gold nanoparticles with immobilized antibodies deposited on glassy carbon electrodes could be used for the immune-sensing detection of botulinum neurotoxin protein absorption [103]. Afkhami et al. reported graphene and gold nanoparticles on chitosan, which was constructed as an impedimetric immune sensor for the immunoassay of botulinum neurotoxin [104].

Ohno and colleagues reported a graphene transistor fabricated with immobilized antibodies of immunoglobulin E (IgE) aptamers on the graphene surface with 1-pyrenebutanoic acid succinimidyl ester as a linker; the electrical conductance of the transistor gate was modified by the adsorption of target proteins [105,106]. They also reported that DNA hybridization could be detected by the change in the electrical

conductance of the graphene transistor [107].

Wang *et al.* reported that an antibody-functionalized gold-gated AlGaN/GaN high electron mobility transistor could detect the adsorption of botulinum neurotoxin proteins by measuring the electrical conductance of the transistor [108]. Yu *et al.* reported label-free prostate-specific antigen (PSA) detection with an AlGaAs/GaAs transistor [109].

Chen *et al.* prepared a potentiometric sensor using a junction-less nanowire transistor with modification of the separated gate by biotin; the transistor was demonstrated to detect streptavidin (SA) [110].

There are many examples changes in electrical conductance by the binding of antigens and immobilized antibodies. Such biosensors are categorized into amperometric detection biosensors.

4-2. Biomedical large-scale integrated circuits for home healthcare and telemedicine

4-2-1. BioCMOS implementation

The development and improvement of portable diagnostic inspection systems that anyone can operate anywhere to obtain immediate results are required to facilitate home healthcare and telemedicine during the COVID-19 pandemic. The integration of biochemistry on a chip, BioCMOS, where several biochemical reactions are controlled and detected electrically, is a key technology for these systems.

Electrochemical biosensors are devices that combine a biological component (a recognition part) and a physicochemical detector component (a transducer). The recognition part can be constructed using enzymes, antibodies, cells, tissues, nucleic acids, and peptide nucleic acids. The transducer consists of potentiometric, amperometric, and impedimetric sensor circuits. The electrical potential, current, and impedance have their own advantages and disadvantages in sensing, and provide complementary information on biomolecules.

One of the design principles of the BioCMOS sensor array is that the structure must be compatible with standard CMOS integrated circuits to supply stable, uniform, and low-price chips [111]. The Nakazato group uses the 150 mm, 0.6-µm, 2-polysilicon, 3-metal mixed signal CMOS process of the Taiwan Semiconductor Manufacturing Company, Limited (TSMC). Gold is a standard electrode material used in electrolyte solutions because of the low ionization tendency and the formation of self-assembled monolayers through thiols. However, gold cannot be introduced into the standard CMOS process, because it creates deep-level electron traps in silicon. As shown in Fig. 13, post-CMOS processes to form gold electrodes, hexamethyldisiloxane (HDS)

passivation layers, polyimide protection layers, and epoxy-based negative photoresist. SU-8 microfluidics were carried out by the MEMS service provider, named MEMS CORE Co., Ltd.

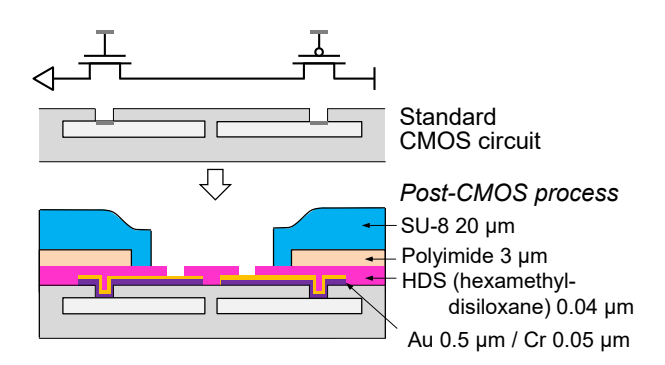


Figure 14. Schematic cross-section of a biosensor fabricated based on CMOS integrated circuits. Gold coating in the post-CMOS process is a key factor for low ionization metal preparation and self-assembled coating of thiols.

Another one of the design principles of the BioCMOS device is that the cell circuits do not influence the system to be detected. Therefore, they have developed several sensor circuits to detect natural chemical reactions that are not disturbed by the sensor circuit [112].

The signal from a biological interaction is quite different from the signal handled in information and technology; therefore, new circuit technologies must be developed. For biological sensing circuits, three principles have been set: operation in the sub-threshold region, current-mode circuits, and time-domain signal representation. Several new circuits have thus been developed, such as the current-mode analog-to-digital converter (ADC).

4-2-2. Potentiometric sensor array

The detection of changes in electrical potential based on a field-effect transistor (FET) has shown excellent sensitivity for the detection of, for example, ion concentration and specific DNA sequences [113]. There are two detection principles for such sensors.

One principle is the detection of electronic charge around an electrode with no electron transfer to the electrode [114]. This method is referred to as direct charge detection. The gate potential is determined by Poisson's equation. However, the direct charge detection method using a FET has a number of serious problems. First, the molecular charge is screened by ions in solution. Second, the charge distribution is influenced by the shape of the molecules. Third, the electrode enters a floating state, so that embedded charge causes a large variation in the threshold voltage.

The other principle is the detection of chemical equilibrium potential, i.e., redox potential, accomplished by electron exchange between the electrolyte/molecule and the electrode [115]. A gold electrode is used to detect an enzyme reaction through a redox reaction. In this case, the gate potential E is determined by the Nernst equation, given by $E = E_0 - \frac{RT}{zF} \ln \frac{[\text{Red}]}{[\text{Ox}]}$, where E_0 is the standard potential, R is the standard gas constant, T is temperature, z is the ion charge, and F is the Faraday constant. [Red] and [Ox] are the molar concentrations of reductant and oxidant, respectively. For example, ferrocene (Fe(II)) is oxidized to ferrocenium_ion (Fe(III)) with a change in the redox potential of approximately 0.4 eV by one electron transfer. In electrochemistry, the potential is closely related with the reduction potential of the reaction.

An enzyme sensor array with a redox mediator using a ferrocenyl-alkanethiol modified gold electrode (Fig. 15) was used to successfully detect a human serum glucose level with an accuracy of 0.2 mg/dL, as shown in Fig. 16(a) [116]. In this case,

three enzymes, hexokinase, glucose-6-phosphate dehydrogenase (G-6-PDH), and diaphorase, were immobilized on beads. The enzyme beads were supplied to the electrodes modified with self-assembled ferrocenyl-alkanethiol monolayers. Figure 16(b) shows the detection signals when glucose, galactose, and maltose samples were supplied, showing no sensitivity to galactose and maltose, which are typically contained in human blood and cause interference in conventional glucose sensors.

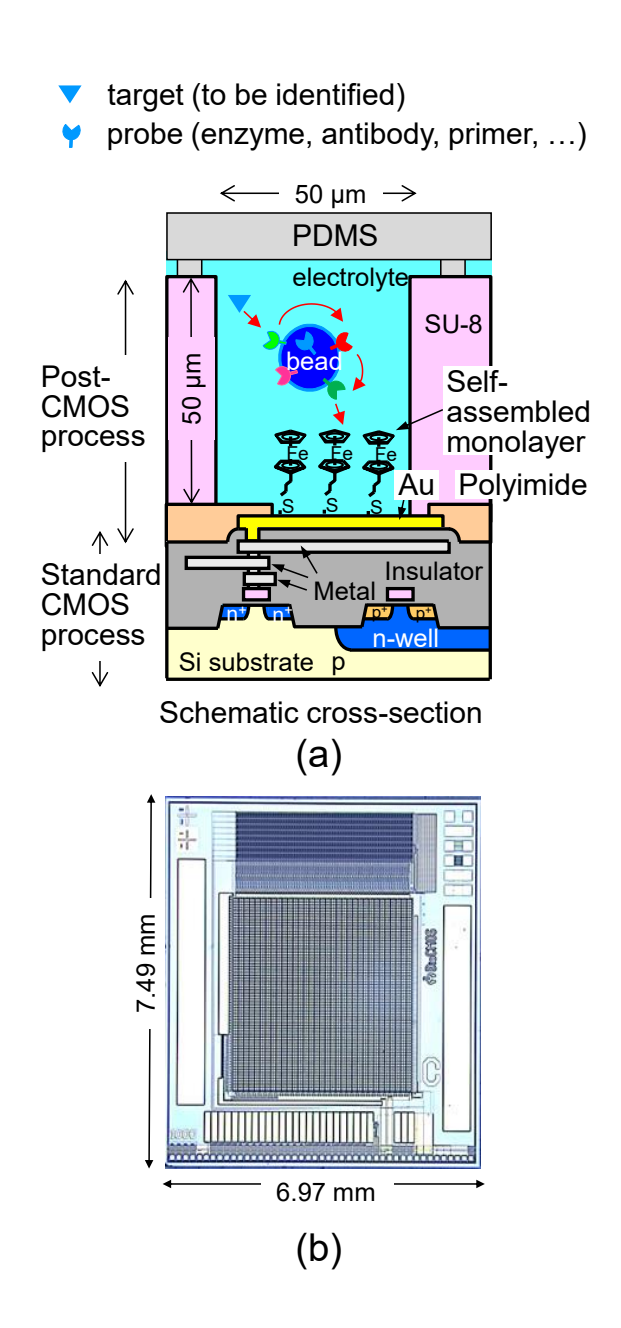


Figure 15. Redox potential sensor array chip. (a) Schematic cross-section and (b) microscopic photograph of the enzyme sensor array.

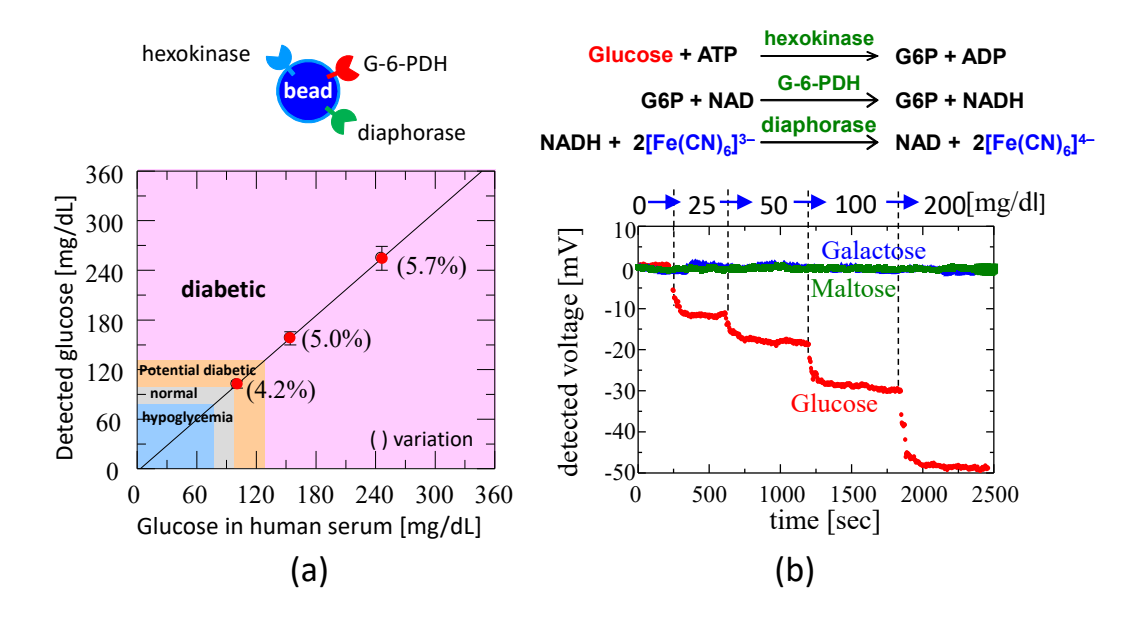


Figure 16. Detection of glucose using an enzyme sensor with redox mediator.

4-2-3. Impedimetric sensor array

An on-chip impedimetric sensor array has been designed that measures impedance at frequencies up to 1 MHz, as shown in Fig. 17. A sensor unit cell consists of two electrodes and selection switches. Even when a sensor cell is unselected, the electrode voltage is kept the same so as not to change the condition around the electrode [117]. The Nakazato group attempted to develop several smart sensor cells in which front-end sensor circuits are formed inside a sensor unit cell to reduce parasitic effects. Although higher frequency operation became possible, the transistor subthreshold voltage variation caused large effects because of the limited cell size, so the smart sensor cell was abandoned. The connection line between electrode and array peripheral circuit is covered by guard layers using upper and lower metals to reduce parasitic capacitance. The voltages at the electrodes in the sensor unit cell are applied by a sinusoidal wave that is generated by an oscillator in the peripheral circuit, and the alternating currents, i_1 and i_2 , are detected by the differential amplifier. The current difference, $i_1 - i_2$, is obtained by a current difference circuit (cDiff), demodulated by a current mode mixer (cMIX), integrated and converted to time by a current mode Δ - Σ analog to time converter (cATC), and output as a 14-bit digital signal by a time-to-digital converter (TDC).

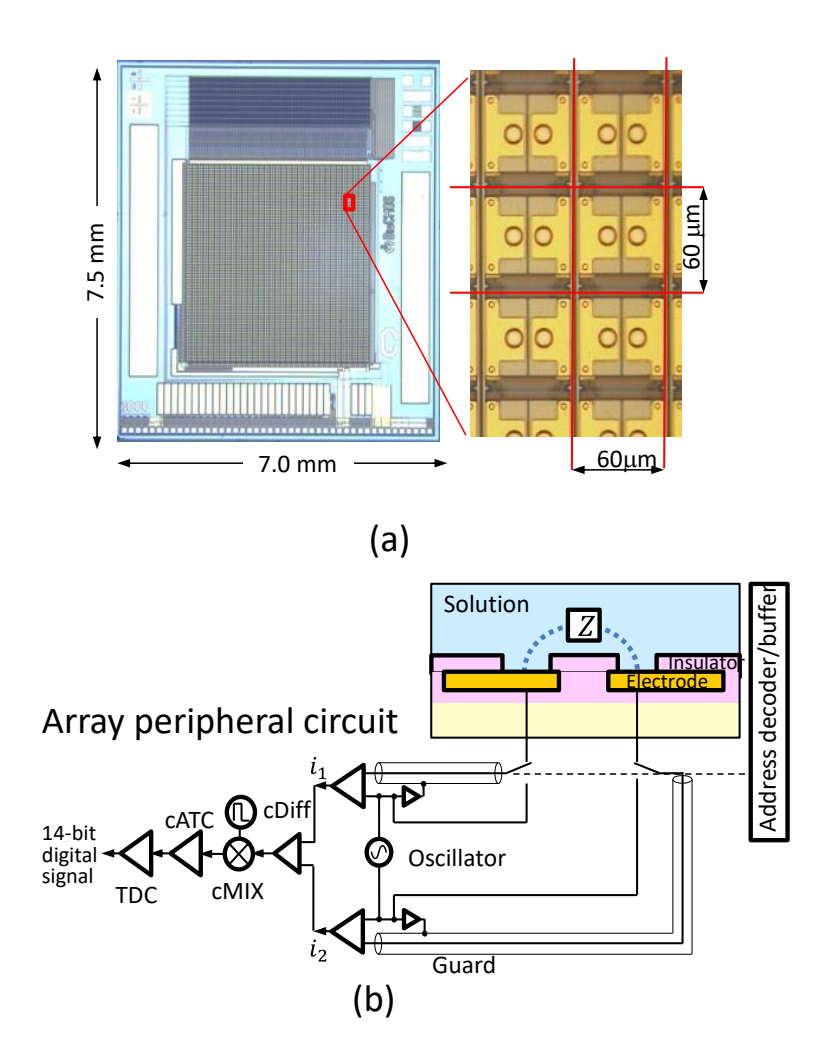


Figure 17. 64×64 impedimetric sensor array. (a) Microscopic photograph array and (b) circuit diagram of the sensor array.

One of the applications of the impedimetric sensor array is the direct counting of viruses or bacteria. There are two detection principles. One principle is the detection of β -dielectric dispersion. Experimentally, dielectric responses appear over various frequency ranges and a dielectric loss spectrum is characterized into two ranges, where one is due to a slow relaxation process, known as α -dispersion, at lower frequency, while the other is a fast relaxation process known as β -dispersion, at higher frequencies, especially in the megahertz range. A virus or bacterium takes a shell structure; therefore, dielectric polarization of an intercellular fluid changes the permittivity at a specific

frequency around the range from 100 kHz to 1 MHz. The other principle is the geometrical effect. When viruses or bacteria are located on the electrode, a part of electrode is covered, so that the resistance increases and capacitance decreases.

Figure 18 shows experimental results. In Fig. 18(a), the β -dielectric dispersion is clearly observed with living *E. coli*. On the other hand, no change is observed in the case of dead *E. coli* and polystyrene beads, because there is no shell structure. In Fig. 18(b), a reduction of conductance (the real part of admittance *Y*) and capacitance (*C*) is observed due to the presence of only a few *E. coli*.

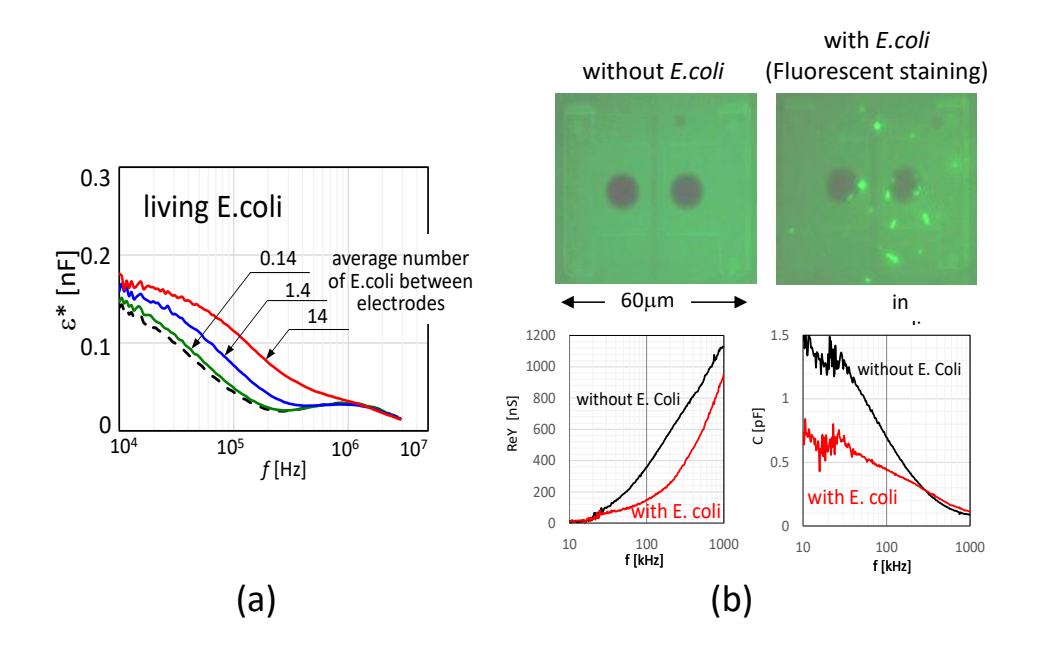


Figure 18. Detection of *Escherichia coli*, O157:H7 ATCC 43888 with BioCMOS devices. (a) Frequency dispersion curves responded to attachment of *E. coli* on the BioCMOS and (b) fluorescent microscopic photograph and impedimetric results.

BioCMOS devices can thus be used to successfully detect adsorbed biological matter by both potentiometric and impedimetric principles. There are many other publications on BioCMOS-related technologies [118-134]. Any bio-sensing system can be designed on the CMOS fabrication platform using three detection principles:

potentiometric (direct current (dc) voltage), amperometric (dc current), and impedimetric (frequency-dependent impedance) detection.

4-3. Vital sign monitor

A stent flow sensor using MEMS technology to measure airflow in the airways of laboratory animals was developed by the Shikida group. When a sensor-wearing subject is breathing, a respiration signal can be taken by an airflow waveform of each exhalation and inhalation due to lung motion and heartbeat. Both respiration and heart functions can be physically diagnosed by connecting these signals. The tube flow sensor is fabricated using MEMS technology and works based on a thermal principle. The stent flow sensor is fabricated by integration of the flow sensor in the center of the tube in the stent structure. The stent structure was first produced by photolithography and wet etching. It was confirmed that the airflow in the airway of a rat could be detected in the sensor output. The response of the sensor signals showed the flow rate in the flow detection characteristics. Furthermore, application of Fourier transform analysis enabled the respiration and heartbeat signals to be successfully identified from the airflow waveform [135-137].

Respiration is one of the important vital signs; however, respiration can be controlled consciously. Subjects that can hold their breath consciously for a short time can thereby suspend and resume respiration easily; therefore, it is difficult to measure the natural respiration condition of such subjects. Sasaki and colleagues developed a wearable respiration sensor for noninvasive vital sign monitoring [138-140]. They put conductive textile electrodes on the abdomen and back of a subject and measured the electrical capacitance formed around the human body. Respiration induces skin contraction and expansion, resulting in capacitance change. Therefore, inhalation and exhalation signals could be acquired from the capacitance measurement. Such wearable sensors do not disturb the subject; therefore, natural respiration can be measured.

Lukas *et al.* suggested that relationships among contact tracing, quarantine, and sterilization protocols could be managed by telemedicine or mobile health (mHealth) to reduce the potential spread of disease and prevent overloading of the healthcare system by at-home COVID-19 screening, diagnosis, and monitoring [141]. In short, the development of a telemetric system that consists of biosensors is essential.

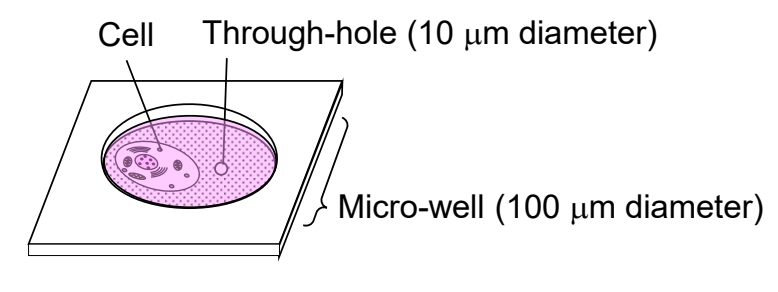
4-4. Future technologies for analysis of infectious disease

After recovery from COVID-19 infection, there have been reports that some of the recovered have suffered from after effects [142,143]. An after-effect is a secondary disease where symptoms can become more serious. At the present time, we have to rely on symptomatic treatments. To overcome COVID-19 and expand the approach to infectious disease in a broad sense, we have to understand how a virus affects human beings and find a solution to stop the activity of a virus in a living body.

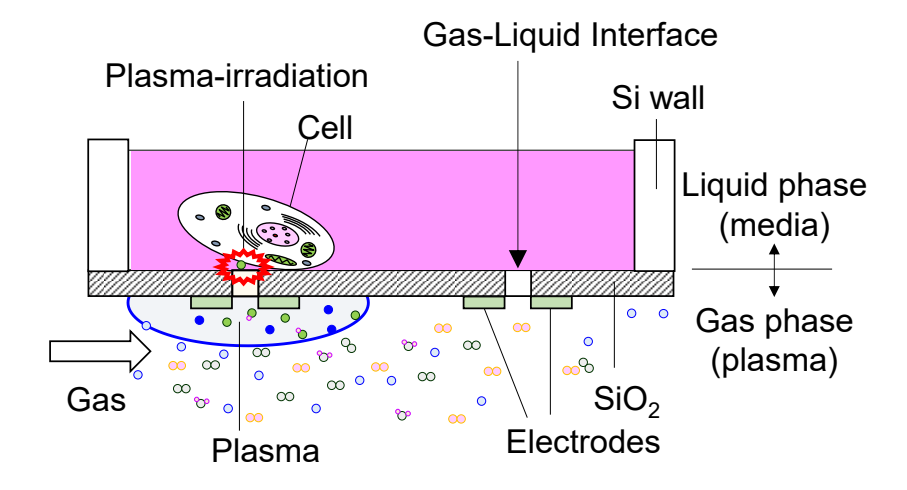
In the field of MEMS, there is a concept of Lab-on-a-Chip. The Lab-on-a-Chip uses microanalytical systems fabricated on a chip. Such microdevice systems can be referred to as a μ-TAS. Cultured cells are one of the hot topics in the fields of Lab-on-a-Chip and μ-TAS. Researchers in the field have constructed an organ model on a chip (organ-on-a-chip) and body structure model on a chip (body-on-a-chip) [144,145]. Kamei *et al.* integrated heart and cancer cells on a chip and reproduced the side effects of anti-cancer drugs [146]. These organ-on-a-chip and body-on-a-chip devices fulfill the 3R principle and will play important roles in the analysis of infectious disease.

It is well known that cells are affected by external stimuli. A plasma can generate complex stimuli by the combination of physical and chemical effects of active species such as chemical, electrical, and optical species. The roles of chemically active species in plasma, such as RONS, have been well investigated to date. There is the possibility that other active species or synergistically active species could affect the viability of a cell. Therefore, plasma-bio researchers are attempting to elucidate the mechanism how plasma affect cells. Kumagai *et al.* developed a microdevice that enables direct plasma irradiation to a cultured cell. The microdevice was referred to as *Plasma-on-Chip* [146,147]. The *Plasma-on-Chip* used a micro air-liquid interface for

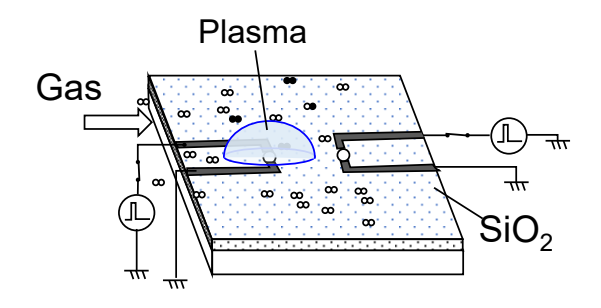
direct plasma irradiation to a cultured cell, as shown in Fig. 19. This device consists of microwells (100 μm×100 μm, 200 μm depth) for cell culture and a micro plasma source to generate nonthermal atmospheric pressure plasma. 10 µm diameter through-holes were fabricated at the bottom of the microwells. When culture medium containing a cell is poured onto a microwell, the surface tension of the liquid medium creates an air-liquid interface at the through-holes. Therefore, the liquid medium is held in a microwell and a cell can be cultured. Next, nonthermal atmospheric pressure plasma is generated by the microplasma source fabricated on the backside of the microwell. The plasma-generated active species pass through the air-liquid interface at the through-hole and directly reach the cell. This direct plasma irradiation enables analysis of the effects of short-lived active species, such as ·OH [148]. Taking advantage of the differences in diffusion length in the liquid medium, it is possible to select the type of active species supplied to the cell using the one of the through-holes for active species delivery. The Plasma-on-Chip device was applied for microorganisms, plant cells [147,148], and animal cells. The *Plasma-on-Chip* technology has opened up a new interdisciplinary research field.



Viewed over micro-well



Cross-section of "Plasma-on-Chip"



Viewed over plasma source

Figure 19. Schematic diagrams of Plasma-on-Chip.

5. Conclusions

This review has provided discussion regarding the contribution of plasma, nanotechnology, and semiconductor devices to overcome infectious disease. First, the sterilization technologies using UV light sources, excimer lamps and DUV-LEDs were reviewed. Shorter wavelengths than 230 nm in the UV-C range can minimize skin damage due to the limited penetration depth for human skin. The development of DUV-LEDs has been extremely fast; however, the current status has just reached the achievement of 276 nm wavelength LEDs. Further engineering of DUV-LEDs is still required and feasible solutions for DUV-LEDs should be explored.

Second, sterilization technologies using low-temperature plasma were reviewed. In addition to UV radiation effects, RONS are effective to chemically inactivate viral pathogens. Peroxynitrite ONOO, dinitrogen pentoxide N₂O₅, and other short-lived species have received much attention recently as substances that can inactivate viruses. The plasma-based sterilization provides an effective tool for both airborne viruses and viruses on substrates.

In addition to sterilization, preventive technologies should be developed with a focus on the detection of infectious viruses. Basically, infection occurs due to virus transmission from an infected to a susceptible person through airborne aerosols, and the direct or indirect touching of fomites. In the surrounding environment of these persons, infectious viruses can be recognized by characterization of their morphology and properties. Filtration with membrane filters and antiviral coating technologies were reviewed.

Moreover, predictive approaches were discussed. To realize diagnostic systems, various types of biosensing technologies are suggested. This topic deals especially with

transducing bio-sensing signals into electrical signals. The biosensing principles are an essential part of realizing such predictive measures. In this review, we have focused on methods to predict infectious diseases before they spread. One approach is biosensing methods with nanomaterials. Antigen-immobilized nanoparticles have potential for the detection of infectious viruses. The other is the system integration of remote diagnostics and telemetry with these biosensors. We emphasize that the term biosensor indicates a combined system of sensing devices, transducers, and ICT-edge functions. BioCMOS technology can be used in a wide variety of designs with potentiometric and impedimetric sensing principles. The leading edge technologies in the semiconductor industry are providing the means with which to fabricate telemetric healthcare monitors. MEMS technology also plays a key role in the health monitoring requirements. In this review, some vital sign monitors were reviewed.

The future sensor networks are developed further, we will be able to predict trends in society. To support this endeavor of the prediction of infectious disease before they spread requires the state of the art of information and communication technology. As biosensors are developed and spread ubiquitously, signal transduction into electrical signals and delivered to the cloud data servers, whereby Bayesian inference and artificial intelligence software will find predictive solutions (Fig. 20). In light of such developments, we should emphasize the importance of more collaborative research among fields such as plasma, materials science, and solid-state physics.

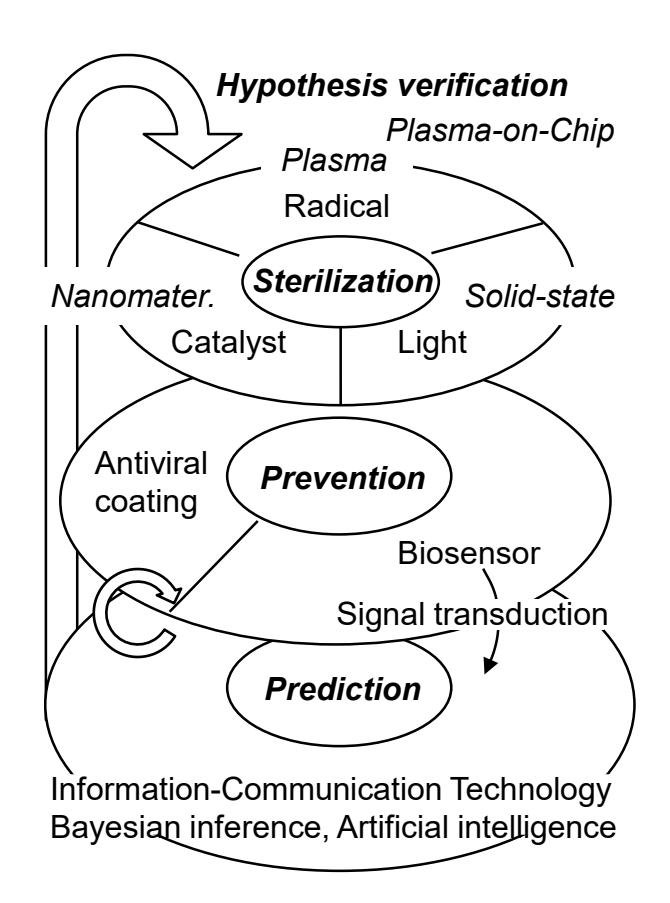


Figure 20. Novel technologies described here are promising solutions for the sterilization, prevention, and prediction of infectious diseases with highly collaborative research over wide areas involving physical plasma technology, solid-state physics, and nanotechnology.

After the global financial crisis in 2010, El-Erian said regarding navigation toward a new normal society that "Having averted a crisis-induced depression, industrial countries are now losing the recovery momentum. To minimize these risks, industrial country societies must go beyond thinking of what to do; they must also consider the how and why. Absent such a shift, active inertia will continue to dominate, instrument innovation will become even more elusive, and the private sector will continue to respond through higher self-insurance and greater deleveraging" [150]. We hope to emerge an innovative technology.

In accordance with such a discussion, a future technology for the analysis of infectious dieses at the cellular level is required. The future technology should maintain the 3R principles—replacement, reduction, and refinement—with respect to animal experiments. The principles promote the rapid development of Lab-on-a-Chip and μ-TAS devices, Among the devices, the *Plasma-on-Chip* devices is increasing in importance with respect to the analysis of interactions between plasmas and biological bodies.

The novel technologies described here are promising solutions for the sterilization, prevention, and prediction of infectious diseases that will advance with highly collaborative research over wide research areas involving physical plasma technology, solid-state physics, and nanotechnology.

Acknowledgements

P. Bruggeman acknowledges all collaborators and researchers who contributed to the work performed at the University of Minnesota during the last few years including S. Al-Sohaimy, A. Andrews, Y. Aranda Gonzalvo, A. Armien, J. Collins, S. Dabhole, U. Gangal, L.A. Higgins, I. Marabella, S.K. Mor, K.V. Nagaraja, M. Nisar, F. Sampedro, M.N. Youssef, and P. Williams.

P. B. declares that this material is partly based upon work supported by the Agriculture and Food Research Initiative of the USDA's National Institute of Food and Agriculture (Grant No. 2017-67017- 26172), by the US Department of Energy, Office of Science, Office of Fusion Energy Sciences General Plasma Science program under Award Number DE-SC-0016053, and by the National Science Foundation (Grant No. PHY 1903151).

K. N. declares that this research was financially supported by the Adaptable and Seamless Technology Transfer Program through Target-driven R&D (No. AS272S001b) from the Japan Science and Technology Agency.

S. K. declares that a part of this study was supported by Kakenhi Grants-in-Aid (Scientific Research (B) 19H04457; Challenging Exploratory Research 18K19942, 26600130) from the Japan Society for the Promotion of Science (JSPS), The Uehara Memorial Foundation, The Nitto Foundation, and Nanotechnology Platform, Toyota Technological Institute Hub, MEXT.

K. I. declares that this research was partly supported by Kakenhi Grants-in-Aid (Nos. 19H05462, 17H02805, 20H00142, and 21H04451) from JSPS, and the Center for Low-temperature Plasma Science, Nagoya University; and by JST COI Grant number JPMJCE1317.

The authors would like to thank professors Dr. Masafumi Ito, Dr Tatsu Shirafuji, and Dr Hiromasa Tanaka and all the members of the program committee of the 13th International Symposium on Advanced Plasma Science and its Applications for Nitrides and Nanomaterials, and the 14th International Conference on Plasma-nanotechnology and Science (ISPlasma2021/IC-PLANTS2021). We also thank Profs. Dr Masaru Hori, Dr Noriyasu Ohno, Dr Hirotaka Toyoda, Dr Masahru Shiratani, Dr Masaaki Mizuno, Dr Keiji Imoto, Dr Shinya Toyokuni, Dr Minoru Fujii, Dr Tetsuo Kachi, Dr Kazuhiro Ohkawa, Dr Yasuo Koide, Dr Thomas von Woedtke for fruitful discussion.

References

- [1] N. J. Rowan, and J. G. Laffey, "Challenges and solutions for addressing critical shortage of supply chain for personal and protective equipment (PPE) arising from Coronavirus disease (COVID19) pandemic Case study from the Republic of Ireland ", Science of the Total environment, 725, 138532 (2020).
- [2] Three Cs https://www.mhlw.go.jp/content/3CS.pdf (last accessed on May 2021)
- [3] World Health Organization "diseases" https://www.who.int (last accessed on April, 2021).
- [4] Navy Environmental Health Center, Ultraviolet Radiat. Guide (1992).
- [5] K. Ishikawa, and M. Hori, "Physical and Chemical basis of nonthermal plasma" In "Plasma medical science", (Academic Press, 2018).
- [6] Excimer lamp https://www.ushio.co.jp (last accessed May 2021).
- [7] J. L. Bezzant, Penetration of human skin by ultraviolet light, https://library.med.utah.edu/kw/derm/ (last accessed May 2021)
- [8] H. A. Aboubakr, U. Gangal, M. M. Youssef, S. M. Goyal, and P. J. Bruggeman, "Inactivation of virus in solution by cold atmospheric pressure plasma: Identification of chemical inactivation pathways," J. Phys. D Appl. Phys., 49, 204001 (2016).
- [9] Z. Chen, G. Garcia, V. Arumugaswami, and R. E. Wirz, "Cold atmospheric plasma for SARS-CoV-2 inactivation", Phys. Plasma 32, 111702 (2020).
- [10] S. Bekeschus, "Gas plasma technology-an asset to healthcare during viral pandemics such as the COVID-19 crisis?" IEEE Trans. Radiation and Plasma Medical Sciences 4, 391 (2020).
- [11] H. Mohamed, G. Nayak, N. Rendine, B. Wigdahl, F. Krebs, P. J. Bruggeman and V. Miller, Non-thermal plasma as a novel strategy for treating or preventing viral infection and associated disease, Frontiers in Physics (2021) in press doi: 10.3389/fphy.2021.683118
- [12] K. Takeda, H. Yamada, K. Ishikawa, H. Sakakita, J. Kim, M. Ueda, J. Ikeda, Y. Akimoto, Y. Kataoka, N. Yokoyama, Y. Ikehara, and M. Hori, "Systematic diagnostics of the electrical, optical, and physicochemical characteristics of

- low-temperature atmospheric-pressure helium plasma sources", J. Phys. D: Appl. Phys. 52, 165202 (2019).
- [13] H. Uchiyama, K. Ishikawa, Q-L. Zhao, G. Andocs, N. Nojima, K. Takeda, M. Krishna, T. Ishijima, Y. Matsuya, M. Hori, K. Noguchi, and T. Kondo, "Free radical generation by non-equilibrium atmospheric pressure plasma in alcohol-water mixtures. An EPR-spin trapping study", J. Phys. D: Appl. Phys. 51, 095202 (2018).
- [14] S. Reuter, and K. Ishikawa, "Plasma chemistry of reactive species in gaseous phase" In "Plasma medical science", (Academic Press, 2018).
- [15] N. Kurake, H. Tanaka, K. Ishikawa, K. Takeda, H. Hashizume, K. Nakamura, H. Kajiyama, T. Kondo, F. Kikkawa, M. Mizuno, and M. Hori, "Effects of ·OH and ·NO radicals in the aqueous phase on H₂O₂ and NO₂ synthesized in plasma-activated medium", J. Phys. D: Appl. Phys. 50, 155202 (2017).
- [16] Narita, K., K. Asano, Y. Morimoto, T. Igarashi and A. Nakane PLoS One 13, e0201259 (2018).
- [17] Nakane, H., S. Takeuchi, S. Yuba, M. Saijo, Y. Nakatsu, H. Murai, Y. Nakatsuru, T. Ishikawa, S. Hirota, Y. Kitamura and et al. Nature 377, 165-168(1995).
- [18] Bradford, P. T., A. M. Goldstein, D. Tamura, S. G. Khan, T. Ueda, J. Boyle, K. S. Oh, K. Imoto, H. Inui, S. Moriwaki, S. Emmert, K. M. Pike, A. Raziuddin, T. M. Plona, J. J. DiGiovanna, M. A. Tucker and K. H. Kraemer, J Med Genet 48, 168-176 (2011).
- [19] Yamano N, Kunisada M, Kaidzu S, Sugihara K, Nishiaki-Sawada A, Ohashi H, Yoshioka A, Igarashi T, Ohira A, Tanito M, Nishigori C, "Long-term effects of 222-nm ultraviolet radiation C sterilizing lamps on mice susceptible to ultraviolet radiation" Photochem Photobiol 96, 853-862 (2020).
- [20] Matsunaga, T., K. Hieda and O. Nikaido Photochem Photobiol 54, 403-410 (1991).
- [21] Fukui, Nishigori, et al. "Exploratory clinical trial on the safety and bactericidal effect of 222-nm ultraviolet C irradiation in healthy humans", PloS One 15, e0235948 (2020).
- [22] Yamano, "Evaluation of acute reactions on mouse skin irradiated with 222 and 235 nm UV-C", Photochem Photobiol (2021) doi: 10.1111/php.13384
- [23] Yamano, "Long-term effect of 222-nm ultraviolet lamp on mice highly susceptible

- to developing ultraviolet-induced skin tumors", Journal Of Investigative Dermatology 139, S126 (2019).
- [24] M. Buonanno, D. Welch, I. Shuryak, and D. J. Brenner, "Far-UVC light (222 nm) efficiently and safely inactivates airborne human coronaviruses", Sci. Rep. 10, 10285 (2020).
- [25] H. Kitagawa, T. Nomura, T. Nazmu, K. Omori, N. Shigemoto, T. Sakaguchi, and H. Ohge, "Effectiveness of 222-nm ultraviolet light on disinfecting SARS-CoV-2 surface contamination", American Journal of Infection Control, 49, 299 (2021).
- [26] M. Buonanno, D. Welch, and D. J. Brenner, "Exposure of human skin models to KrCl excimer lamps: the impact of optical filtering", Photochem Photobiol 97, 517 (2021).
- [27] E. Eadie, I. M. R. Barnard, S. H. Ibbotson, K. Wood, "Extreme exposure to filtered far-UVC: A Case Study", Photochem Photobiol 97, 527 (2021).
- [28] M. Hessling, R. Haag, N. Sieber, and P. Vatter, "The impact of far-UVC radiation (200-230 nm) on pathogens, cells, skin, and eyes a collection and analysis of a hundred years of data", GMS Hygiene and Infection Control, (2021) doi: 10.3205/dgkh000378
- [29] H. Amano et al., J. Phys. D: Appl. Phys. 53, 503001 (2020).
- [30] Y. Narukawa, M. Ichikawa, D. Sanga, M. Sano and T. Mukai, J. Phys. D: Appl. Phys. 43, 354002 (2010).
- [31] J. Simon, V. Protasenko, C. Lian, H. Xing, and D. Jena, Science, 327, 60 (2010).
- [32] T. Takeuchi, S. Kamiyama, M. Iwaya and I. Akasaki, Semicond. Sci, Technol., 36, 063001 (2021).
- [33] O. B. Shchekin,a_ J. E. Epler, T. A. Trottier, T. Margalith, D. A. Steigerwald, M. O. Holcomb, P. S. Martin, and M. R. Krames, Appl. Phys. Lett., 86, 071109 (2006).
- [34] S. Liu, et al. "Sec-eliminating the SARS-CoV-2 by AlGaN based high power deep ultraviolet light source". Adv. Funct. Mater. 31, 2008452 (2021).
- [35] DUV LED https://www.toyoda-gosei.com/ (last accessed May 2021).
- [36] An overview of collaborative research performed at the University of Minnesota since 2013 is provided here.

- [37] H. Aboubakr, P. Wiliams, U. Gangal, M. Youssef, S. Al-Sohaimy, P. Bruggeman and S. Goyal, Applied and Environmental Microbiology 81, 3612-3622 (2015).
- [38] H. Aboubakr, U. Gangal, M. Youssef, S. Goyal and P. Bruggeman, J. Phys. D: Appl. Phys 49, 204001 (2016)
- [39] H. A. Aboubakr, S. K. Mor, A. Armien, L A. Higgins, M. M. Youssef, P. J. Bruggeman and S. M. Goyal, PLOS one, 13, e0194618 (2018).
- [40] J. Jiang, Y. Aranda Gonzalvo and P. J. Bruggeman, Plasma Sources Sci. Technol. 29, 045023 (2020)
- [41] G. Nayak, H. Aboubakr, S. Goyal, P. J. Bruggeman, Plasma Process. Polym. 15, e170119 (2018)
- [42] A. Moldgy, G. Nayak, H. A. Aboubakr, S.M. Goyal and P. J. Bruggeman, J, Phys. D: Appl. Phys. 53, 434004 (2020).
- [43] H. Aboubakr, J. Collins, P. J. Bruggeman, F. Sampedro, and S. Goyal, Food Microbiol., 85, 103307 (2020)
- [44] H. A. Aboubakr, M. Nisar, G. Nayak, K.V. Nagaraja, J. Collins, P. J. Bruggeman and S. M. Goyal, Foodborne Pathogens and Disease, 17, 157-165 (2020)
- [45] A. Moldgy, H. Aboubakr, G. Nayak, S. Goyal and P. Bruggeman, Plasma Process. Polym. 17, e1900234 (2020)
- [46] G. Nayak, A. Andrews, I. Marabella, H.Aboubakr, S. M. Goyal, B. Olson, M. Torremorell and P. J. Bruggeman, Plasma Process. Polym. 17, e1900269 (2020)
- [47] Y. Kimura, K. Takashima, S. Sasaki and T. Kaneko: J. Phys. D: Appl. Phys. 52, 064003 (2019).
- [48] K. Shimada, K. Takashima, Y. Kimura, K. Nihei, H. Konishi, and T. Kaneko: Plasma Process. Polym. 17, e1900004 (2020).
- [49] A. Ochi, H. Konishi, S. Ando, K. Sato, K. Yokoyama, S. Tsushima, S. Yoshida, T. Morikawa, T. Kaneko, and H. Takahashi, Plant Pathology 66, 67 (2016).
- [50] S. E. Hanbal, K. Takashima, S. Miyashita, S. Ando, K. Ito, M. M. Elsharkawy, T. Kaneko, and H. Takahashi, Arch. Virol. 163, 2835 (2018).
- [51] S. Sasaki, K. Takashima and T. Kaneko, Ind. Eng. Chem. Res. 60, 798 (2020).

- [52] K. Takashima, Y. Hu, T. Goto, S. Sasaki, and T. Kaneko, J. Phys. D: Appl. Phys. 53, 354004 (2020).
- [53] The NBP sources were developed and used in Plasma Bioscience Research Center (PBRC).
- [54] J. S. Lim, Y. J. Hong, B. Ghimire, J. S. Choi, S. Mumtaz, E. H. Choi, Results in Physics 20, 103693 (2021).
- [55] P. Attri, Y. H. Kim, D. H. Park, J. H. Park, Y. J. Hong, H. S. Uhm, K-N. Kim, A. Fridman, and E. H. Choi., "Generation mechanism of hydroxyl radical species and its lifetime prediction during the plasma-initiated ultraviolet (UV) photolysis", Sci. Rep. 5, 9332 (2015).
- [56] X. Lu, M. Keidar, M. Laroussi, E. Choi, E.J. Szili, and K. Ostrikov, Materials Science & Engineering R 138, 36 (2019).
- [57] Y. J. Hong, J. Lim, J. S. Choi, K. D. Weltmann, and E. H. Choi, "Measurement of nitrogen dioxide and nitric oxide densities by using CEAS (cavity-enhanced absorption spectroscopy) in nonthermal atmospheric pressure air plasma", Plasma Process Polym.18, 2000168 (2021).
- [58] C. H. Song, P. Attri, S. K. Ku, I. Han, A. Bogaerts, and E. H. Choi, "Cocktail of reactive species generated by cold atmospheric plasma: oral administration induces non-small cell lung cancer cell death", J. Phys. D: Appl. Phys. 54, 185202 (2021).
- [59] T. H. Choi, H. B. Park, "Membrane and virus filter trends in the processes of biopharmaceutical production", Membrane Journal 30, 9 (2020).
- [60] K. Priyam Goswami, and G. Pugazhenth "Credibility of polymeric and ceramic membrane filtration in the removal of bacteria and virus from water: A review", Journal of Environmental Management 268 (2020) 110583.
- [61] H. Yukawa, S. Yamazaki, K. Aoki, K. Muto, N. Kihara, K. Sato, D. Onoshima, T. Ochiya, Y. Tanaka, and Y. Baba, "Co-continuous structural effect of size-controlled macro-porous glass membrane on extracellular vesicle collection for the analysis of miRNA", Scientific Reports 11, 8672 (2021).
- [62] D. Onoshima, Y. Hattori, H. Yukawa, K. Ishikawa, M. Hori, and Y. Baba, "Cell deposition microchip with micropipette control over liquid interface motion", Cell Medicine 10, 1 (2018).

- [63] N. Kihara, H. Odaka, D. Kuboyama, D. Onoshima, K. Ishikawa, Y. Baba, and M. Hori, "Facile fabrication of a polyethylene terephthalate (PET) membrane filter with precise alignments of through holes", Japan J. Appl. Phys. 57, 037001 (2018).
- [64] N. Kihara, D. Kuboyama, D. Onoshima, K. Ishikawa, R. Koguchi, H. Tanaka, N. Ozawa, T. Hase, H. Yukawa, H. Odaka, Y. Hasegawa, Y. Baba, and M. Hori, "Low-auto fluorescence fluoropolymer membrane filters for cell filtration", Japan J. Appl. Phys. 57, 06JF03 (2018).
- [65] T. Ito, K. Ishikawa, D. Onoshima, N. Kihara, K. Tatsukoshi, H. Odaka, H. Hashizume, H. Tanaka, H. Yukawa, K. Takeda, H. Kondo, M. Sekine, Y. Baba, and M. Hori, "Microfluidic transport through micro-sized holes treated by non-equilibrium atmospheric-pressure plasma", IEEE Transactions on Plasma Science 44, 3060 (2016).
- [66] D. Kuboyama, D. Onoshima, H. Yukawa, H. Tanaka, K. Ishikawa, M. Hori, and Y. Baba, "Micro sand timer in glass membrane device separates single circulating tumor cells in blood", The 20th International Conference on Miniaturized Systems for Chemistry and Life Sciences, Micro Total Analysis Systems 2016, pp. 297-298.
- [67] N. Kihara, "Plasma processes for circulating tumor cells isolation devices", Doctor dissertation (Nagoya University, 2019).
- [68] S. L. Warnes, and C. W. Keevil, "Inactivation of norovirus on dry copper alloy surfaces", PLoS One 9, e98333 (2013).
- [69] Y. Fujimori, T. Sato, T. Hayata, T. Nagao, M. Nakayama, T. Nakayama, R. Sugamata, and K. Suzuki, "Novel antiviral characteristics of nanosized copper(I) iodide particles showing inactivation activity against 2009 pandemic H1N1 influenza virus", Appl. Environ. Microbiol. 78, 951–955 (2012).
- [70] N. Shionoiri, T. Sato, Y. Fujimori, T. Nakayama, M. Nemoto, T. Matsunaga, T. Tanaka, "Investigation of the antiviral properties of copper iodide nanoparticles against feline calicivirus", J. Biosci. Bioeng., 113, 580-586 (2012).
- [71] S. Zerbib, L. Vallet, A. Muggeo, C. de Champs, A. Lefebvre, D. Jolly, and L. Kanagaratnam, "Copper for the prevention of outbreaks of health care—associated infections in a long-term care facility for older adults", J. Am. Med. Dir. Assoc. 21, 68-71 (2020).
- [72] N. van Doremalen, T. Bushmaker, D. H. Morris, M. G. Holbrook, A. Gamble, B. N.

- Williamson, A. Tamin, J. L. Harcourt, N. J. Thornburg, S. I. Gerber, J. O. Lloyd-Smith, E. de Wit, and V. J. Munster, "Aerosol and surface stability of SARS-CoV-2 as compared with SARS-CoV-1", N. Engl. J. Med. 382, 1564 (2020).
- [73] N. Hutasoit, B. Kennedy, S. Hamilton, A. Luttick, R. A. R. Rashid, and S. Palanisamy, "SARS-CoV-2 (COVID-19) inactivation capability of copper-coated touch surface fabricated by cold-spray technology", Manuf. Lett. 25, 93–97 (2020).
- [74] A. Frei, J. Zuegg, A. G. Elliott, et al., "Metal complexes as a promising source for new antibiotics", Chem. Sci. 11, 2627 (2020).
- [75] Y. Mori, T. Ono, Y. Miyahira, V. Q. Nguyen, T. Matsui, and M. Ishihara "Antiviral activity of silver nanoparticle/chitosan composites against H1N1 influenza A virus", Nanoscale Research Letters, 8, 93 (2013).
- [76] S. S. Jeremiah, K. Miyakawa, T. Morita, Y. Yamaoka, A. Ryo, "Potent antiviral effect of silver nanoparticles on SARS-CoV-2", Biochemical and Biophysical Research Communications, 533, 195-200 (2020).
- [77] S. Nakamura, N. Ando, M. Sato, and M. Ishihara, "Ultraviolet irradiation enhances the microbicidal activity of silver nanoparticles by hydroxyl radicals", Int. J. Mol. Sci. 21, 3204 (2020).
- [78] List of textile fibres https://en.wikipedia.org/wiki/List_of_textile_fibres (last accessed may 2021)
- [79] T-T-N. Nguyen, Y-H. Chen, M-Y. Chen, K-B. Cheng, and J-L. He, "Multifunctional Ti-O coatings on polyethylene terephthalate fabric produced by using roll-to-roll high power impulse magnetron sputtering system", Surface and Coatings Technology 324, 249-256 (2017).
- [80] T-T-N. Nguyen, Y-H. Chen, Z-M. Chen, K-B. Cheng, and J-L. He, "Microstructure, near infrared reflectance, and surface temperature of Ti-O coated polyethylene terephthalate fabrics prepared by roll-to-roll high power impulse magnetron sputtering system", Thin Solid Films 663, 1-8 (2018).
- [81] A. Fujishima, and K. Honda, "Electrochemical photolysis of water at a semiconductor electrode", Nature, 238, 37 (1972).
- [82] A. Fujishima, X. T. Zhang, and D. A. Tryk, "TiO₂ photocatalysis and related surface phenomena" Surface Science Reports 63, 515 (2008).

- [83] J. Schneider, M. Matsuoka, M. Takeuchi, J. Zhang, Y. Horiuchi, M. Anpo, and D. W. Bahnemann, "Understanding TiO₂ photocatalysis: mechanisms and materials", Chem. Rev. 114, 19, 9919–9986 (2014).
- [84] M. Miyauchi, H. Irie, M. Liu, X. Qiu, H. Yu, K. Sunada, and K. Hashimoto, "Visible-light-sensitive photocatalysts: nanocluster-grafted titanium dioxide for indoor environmental remediation", J. Phys. Chem. Lett. 7, 75–84 (2016).
- [85] K. Miyaguchi, S. Kajita, H. Tanaka, and N. Ohno, "Fabrication of nanostructured Ti thin film with Ti deposition in He plasmas", Japan. J. Appl. Phys. 60, 038004 (2021).
- [86] S. Kajita, Y. Tomita, E. Yasunaga, T. Yoshida, K. Miyaguchi, H. Tanaka, and N. Ohno, "Photocatalytic decomposition of ethylene using He plasma induced nano-TiO₂", Japan. J. Appl. Phys. 58, 070903 (2019).
- [87] Y. Tomita, S. Kajita, E. Yasunaga, T. Yoshida, and N. Ohno, "Fabrication of a nanostructured TiO₂ photocatalyst using He plasma-irradiated tungsten and ethylene gas decomposition", Japan. J. Appl. Phys. 58, SEEG01 (2019).
- [88] D. Kindole, and Y. Ando, "Application of atmospheric solution precursor plasma spray to photocatalytic devices for small and medium industries in developing countries", Japan. J. Appl. Phys. 56, 01AB10 (2017).
- [89] Y. Kitazawa, J. J. Jia, S. Nakamura, and Y. Shigesato, "Deposition of TiO₂ photocatalyst on polyethylene terephthalate or polyimide polymer films by reactive sputtering for flexible photocatalytic sheets", Japan. J. Appl. Phys. 58, 055503 (2019).
- [90] M. Honda, K. Hizumi, R. I. Devi, N. Tiwari, Y. Saito, and Y. Ichikawa, "Near-UV plasmon resonances for enhanced TiO₂ photocatalysis", Japan. J. Appl. Phys. 59, 045001 (2020).
- [91] S-Y. Feng, S. Kajita, Y. Tomita, T. Yoshida, and N. Ohno, "Photocatalytic application of helium plasma induced nanostructured tungsten oxides", Japan. J. Appl. Phys. 59, AAB04 (2020).
- [92] N. A. Abdullah, N. A. M. Asib, N. A. A. Aziz, S. Z. Umbaidilah, T. Soga, S. A. H. Alrokayan, H. A. Khan, M. R. Mahmood and Z. Khusaimi, " Evaluation of the crystalline structure of Ag⁺-doped ZnO thin film treated with selected annealing temperatures", Japan. J. Appl. Phys. 59, SAAC12 (2020).

- [93] Q. Y. Zhang, M. Honda, and Y. Ichikawa, "Fabrication of ZnS/ZnO composite photocatalysts by spin-coating ZnS nanoparticles on ZnO thin film", Japan. J. Appl. Phys. 60, 036504 (2021).
- [94] H. Masegi, S. Imai, S. B. Sadale, and K. Noda, "All-electrochemical fabrication of alpha-Fe₂O₃ nanotube array/Cu₂O composites toward visible-light-responsive photocatalysis", Japan. J. Appl. Phys. 59, 065503 (2020).
- [95] B. Tanga, J. Wang, S. Xu, T. Afrin, J. Tao, W. Xu, L. Sun, and X. Wang, "Function improvement of wool fabric based on surface assembly of silica and silver nanoparticles", Chemical Engineering Journal 185–186, 366-373 (2012).
- [96] A. D. Chintagunta, S. K. M, S. Nalluru, and S. Kumar N. S., "Nanotechnology: an emerging approach to combat COVID-19", Emergent Materials, 4, 119 (2021).
- [97] M. Zare, M. Zare, J. A. Butler, and S. Ramakrishna, "Nanoscience-led antimicrobial surface engineering to prevent infections", Appl. Nano Mater. (2021) doi: 10.1021/acsanm.1c00466
- [98] N. Misra, S. Bhatt, F. Arefi-Khonsari, and V. Kumar, Plasma Process Polym. (2021) doi: 10.1002/ppap.202000215
- [99] K. Friston, and S. Kiebel, "Predictive coding under the free-energy principle", Philos. Trans. Roy. Soc. B, 264, 1211 (2009)
- [100] E. Törnqvist, A. Annas, B. Granath, E. Jalkesten, I. Cotgreave, and M. Öberg, "Strategic focus on 3R principles reveals major reductions in the use of animals in pharmaceutical toxicity testing", PLOS One 9, e101638 (2014).
- [101] Y. Huang, X. Dong, Y. Liu, L-J. Li, and P. Chen, "Graphene-based biosensors for detection of bacteria and their metabolic activities", J. Mater. Chem. 21, 12358 (2011).
- [102] D. Kim, H-J. Kim, S-B. Shim, S. Jung, N. H. Lee, S. H. Nahm, E-C. Shin, W. S. Yun, and D. H. Ha, "Electrical conductance change of graphene-based devices upon surface modification for detecting botulinum neurotoxin", Japan. J. Appl. Phys. 56, 067001 (2017).
- [103] J. Narayanan, M. K. Sharma, S.Ponmariappan, S. M. Shaik, and S. Upadhyay, "Electrochemical immunosensor for botulinum neurotoxin type-E using covalently ordered graphene nanosheets modified electrodes and gold nanoparticles-enzyme

- conjugate", Biosensors Bioelectronics 69, 249 (2015).
- [104] A. Afkhami, P. Hashemi, H. Bagheri, J. Salimian, A. Ahmadi, and T. Madrakian, "Impedimetic immunosensor for the label-free and direct detection of botulinum neurotoxin serotype A using Au nanoparticles/graphene-chitosan composite", Biosensors Bioelectronics 93, 124 (2017).
- [105] Y. Ohno, K. Maehashi, K. Inoue, and K. Matsumoto, "Label-free aptamer-based immunoglobulin sensors using graphene field-effect transistors", Japan. J. Appl. Phys. 50, 070120 (2011).
- [106] S. Okamoto, Y. Ohno, K. Maehashi, K. Inoue, and K. Matsumoto, "Immunosensors based on graphene field-effect transistors fabricated using antigen-binding fragment", Japan. J. Appl. Phys. 51, 06FD08 (2012).
- [107] Y. Ohno, S. Okamoto, K. Maehashi, and K. Matsumoto, "Direct electrical detection of DNA hybridization based on electrolyte-gated graphene field-effect transistor", Japan. J. Appl. Phys. 52, 110107 (2013).
- [108] Y-L. Wabg, B. H. Chu, K. H. Chen, C. Y. Chang, T. P. Lele, Y. Tseng, S. J. Pearton, J. Ramage, D. Hooten, A. Dabiran, P. P. Chow, and F. Ren, "Botulinum toxin detection using AlGaN/GaN high electron mobility transistors", Appl. Phys. Lett. 93, 262101 (2008).
- [109] J. H. Yu, M. Xu, L. Liang, M. Guan, Y. Zhang, F. Yan, and H. Cao, "Separative extended-gate AlGaAs/GaAs HEMT biosensors based on capacitance change strategy", Appl. Phys. Lett. 116, 123704 (2020).
- [110] C. W. Chen, R-Z. Lin, L-C. Chiang, F-M. Pan, and J-T. Sheu, "Junctionless gate-all-around nanowire field-effect transistors with an extended gate in biomolecule detection", Japan. J. Appl. Phys. 58, 027001 (2019).
- [111] K. Nakazato, "BioCMOS LSIs for portable gene-based diagnostic inspection system", IEEE International Symposium on Circuits and Systems (ISCAS 2012) (2012), p. 2287.
- [112] *CMOS circuits for Biological Sensing and Processing*, ed. by S. Mitra and D. R. S. Cumming, (Springer, 2017).
- [113] J. M. Rothberg, et al. An integrated semiconductor device enabling non-optical genome sequencing. Nature 475, 348–352, (2011).

- [114] P. Bergveld,. "Development of an ion-sensitive solid-state device for neurophysical measurements", IEEE Trans. Biomed. Eng. BME-17, 70–71, (1970).
- [115] Y. Ishige, M. Shimoda, and M. Kamahori. "Extended-gate FET-based enzyme sensor with ferrocenyl-alkanethiol modified gold sensing electrode", Biosens. Bioelectron. 24, 1096–1102, (2009).
- [116] H. Anan, M. Kamahori, Y. Ishige, and K. Nakazato. "Redox-potential sensor array based on extended-gate field-effect transistors with ω-ferrocenylalkane thiol-modified gold electrodes" Sensors and Actuators B: Chemical. 187, 254 (2012).
- [117] J. Hasegawa, S. Uno, and K. Nakazato, "Amperometric electrochemical sensor array for on-chip simultaneous imaging: circuit and microelectrode design considerations", Japan. J. Appl. Phys. 50, 04DL03 (2011).
- [118] K. Gamo, K. Nakazato, and K. Niitsu, "Design and experimental verification of CMOS magnetic-based microbead detection using an asynchronous intra-chip inductive-coupling transceiver", Japan. J. Appl. Phys. 56, 01AH05 (2017).
- [119] K. Niitsu, T. Ando, A. Kobayashi, and K. Nakazato, "Enhancement in open-circuit voltage of implantable CMOS-compatible glucose fuel cell by improving the anodic catalyst", Japan. J. Appl. Phys. 56, 01AH04 (2017).
- [120] K. Niitsu, K. Ikeda, K. Muto, and K. Nakazato, "Design, experimental verification, and analysis of a 1.8-V-input-range voltage-to-current converter using source degeneration for low-noise multimodal CMOS biosensor array", Japan. J. Appl. Phys. 56, 01AH06 (2017).
- [121] A. Kobayashi, K. Ikeda, K. Nakazato, and K. Niitsu, "Energy-efficient and low-voltage design methodology for a supply-sensing CMOS biosensor using biofuel cells for energy-autonomous healthcare applications", Japan. J. Appl. Phys. 56, 01AH03 (2017).
- [122] K. Gamo, K. Nakazato, and K. Niitsu, "Design, theoretical analysis, and experimental verification of a CMOS current integrator with 1.2 x 2.05 mu m² microelectrode array for high-sensitivity bacterial counting", Japan. J. Appl. Phys. 56, 01AH01 (2017).
- [123] K. Gamo, K. Nakazato, and K. Niitsu, "A current-integration-based CMOS amperometric sensor with 1024 x 1024 bacteria-sized microelectrode array for

- high-sensitivity bacteria counting", IEICE Transactions on Electronics E100C, 602 (2017).
- [124] K. Ikeda, A. Kobayashi, K. Nakazato, and K. Niitsu, "Design and analysis of scalability in current-mode analog-to-time converter for an energy-efficient and high-resolution CMOS biosensor array", IEICE Transactions on Electronics E100C, 597 (2017).
- [125] K. Ikeda, A. Kobayashi, K. Nakazato, and K. Niitsu, "Design and electrochemical measurement of a current-mode analog-to-time converter with short-pulse output capability using local intra-cell activation for high-speed time-domain biosensor array", Analog Integrated Circuits And Signal Processing 92, 403 (2017).
- [126] Y. Yamaji, K. Nakazato, and K. Niitsu, "Sub-1-V CMOS-based electrophoresis using electroless gold plating for small-form-factor biomolecule manipulation", IEICE Transactions on Electronics E100C, 592 (2017).
- [127] A. Kobayashi, K. Ikeda, Y. Ogawa, H. Kai, M. Nishizawa, K. Nakazato, and K. Niitsu, "Design and experimental verification of a 0.19 V 53 μW 65 nm CMOS integrated supply-sensing sensor with a supply-insensitive temperature sensor and an inductive-coupling transmitter for a self-powered bio-sensing system using a biofuel cell", IEEE Transactions On Biomedical Circuits And Systems 11, 1313 (2017).
- [128] K. Itakura, K. Kayano, K. Nakazato and K. Niitsu, "Theoretical analysis and simulation study of low-power CMOS electrochemical impedance spectroscopy biosensor in 55 nm deeply depleted channel technology for cell-state monitoring", Japan. J. Appl. Phys. 57, 01AG02 (2018).
- [129] T. Nakanishi, M. Matsunaga, A. Kobayashi, K. Nakazato and K. Niitsu, "A 40 GHz fully integrated circuit with a vector network analyzer and a coplanar-line-based detection area for circulating tumor cell analysis using 65 nm CMOS technology", Japan. J. Appl. Phys. 57, 03EC01 (2018).
- [130] M. Matsunaga, A. Kobayashi, K. Nakazato and K. Niitsu, "Design trade-off between spatial resolution and power consumption in CMOS biosensor circuit based on millimeter-wave LC oscillator array", Japan. J. Appl. Phys. 57, 03EC02 (2018).
- [131] S. Arata, K. Hayashi, Y. Nishio, A. Kobayashi, K. Nakazato, and K. Niitsu, "Wafer-scale development and experimental verification of 0.36 mm² 228 mV

- open-circuit-voltage solid-state CMOS-compatible glucose fuel cell", Japan. J. Appl. Phys. 57, 04FM04 (2018).
- [132] K. Niitsu, A. Kobayashi, Y. Nishio, K. Hayashi, K. Ikeda, T. Ando, Y. Ogawa, H. Kai, M, Nishizwa, and K. Nakazato, "A Self-Powered Supply-Sensing Biosensor Platform Using Bio Fuel Cell and Low-Voltage, Low-Cost CMOS Supply-Controlled Ring Oscillator With Inductive-Coupling Transmitter for Healthcare IoT", IEEE Transactions on Circuits And Systems 65, 2784 (2018).
- [133] M. Matsunaga, T. Nakanishi, A. Kobayashi, K. Nakazato and K. Niitsu, "Design and analysis of a three-dimensional millimeter-wave frequency-shift based CMOS biosensor using vertically stacked spiral inductors in LC oscillators", Analog Integrated Circuits and Signal Processing 98, 453 (2019).
- [134] K. Niitsu, T. Nakanishi, S. Murakami, M. Matsunaga, A. Kobayashi, K. N. Mohammad, J. Ito, N. Ozawa, T. Hase, H. Tanaka, M. Sato, H. Kondo, K. Ishikawa, H. Odaka, Y. Hasegawa, M. Hori, and K. Nakazato, "A 65-nm CMOS fully integrated analysis platform using an on-chip vector network analyzer and a transmission-line-based detection window for analyzing circulating tumor cell and exosome", IEEE Transactions on Biomedical Circuits and Systems 13, 470 (2019).
- [135] H. Noma, Y. Hasegawa, M. Matsushima, T. Kawabe and M. Shikida, "Micro-machined stent flow sensor for detecting breathing and heartbeat from airflow in airway of rat", J. Micromech. Microeng. 31, 025006 (2021).
- [136] Y. Kawamoto, Y. Maeda, Y. Hasegawa, M. Matsushima, T. Kawabe, and M. Shikida, "Development of sensor-probe system with function of measuring flow and pressure for evaluating breathing property at airway in lungs", Microsystem Technologies (2021) doi: 10.1007/s00542-020-05201-0
- [137] A. Kato, Y. Hasegawa, K. Taniguchi, M. Matsushima, T. Kawabe, and M. Shikida, "A micro-machined flow sensor formed on copper on a polyimide substrate and its application to respiration measurement", Japan. J. Appl. Phys. 58, SDDL07 (2019).
- [138] S. K. Kundu, S. Kumagai, and M. Sasaki, "A Wearable Capacitive Sensor for Monitoring Human Respiratory Rate", Japan. J. Appl. Phys. **52**, 04CL05 (2013).
- [139] M. Terasawa, S. Kumagai, M. Sasaki, "Frequency-response-based analysis of respiratory sensor measuring capacitance built across skin", Japan. J. Appl. Phys. 55, 04EM13 (2016).

- [140] M. Terazawa, M. Karita, S. Kumagai, and M. Sasaki, "Respiratory motion sensor measuring capacitance constructed across skin in daily activities", Micromachines 9, 543 (2018).
- [141] H. Lucas, "Emerging telemedicine tools for remote COVID-19 diagnosis, monitoring, and management", ACS Nano 14, 16180 (2020).
- [142] M. Marshall, "The lasting misery of coronavirus long-haulers", Nature **585**, pp. 339-341.
- [143] A. Nalbandian, K. Sehgal, A. Gupta, et al. "Post-acute COVID-19 syndrome", Nat Med 27, 601–615 (2021). https://doi.org/10.1038/s41591-021-01283-z.
- [144] H. Kimura, Y. Sakai, and T. Fujii, "Organ/body-on-a-chip based on microfluidic technology for drug discovery", Drug Metabolism and Pharmacokinetics **33**, 43-48 (2018).
- [145] K.-I. Kamei, Y. Kato, Y. Hirai, S. Ito, J. Satoh, A. Oka, T. Tsuchiy, Y. Chenad, and O. Tabata, "Integrated heart/cancer on a chip to reproduce the side effects of anti-cancer drugs in vitro", RSC Advances 7, 36777-37786 (2017).
- [146] S. Kumagai, C.-Y. Chang, J.-H. Jeong, M. Kobayashi, T. Shimizu, and M. Sasaki, "Development of plasma-on-chip: Plasma treatment for individual cells cultured in media", Jpn. J. Appl. Phys. **55**, 01AF01 (2016).
- [147] T. Okada, C.-Y. Chang, M. Kobayashi, T. Shimizu, M. Sasaki, and S. Kumagai, "Plasma-on-chip device for stable irradiation of cells cultured in media with a low-temperature atmospheric pressure plasma", Archives Biochem. Biophy. **605**, 11-18 (2016).
- [148] S. Kumagai, M. Kobayashi, T. Shimizu, and M. Sasaki, "*Plasma-on-Chip*: device for non-thermal atmospheric pressure plasma irradiation to single cells", Electron Comm Jpn. **103**, 43-48 (2020).
- [149] K. Ishikawa, M. Sasaki, and S. Kumagai, "Measurement of hydroxyl radicals delivered into liquid through a micro gas—liquid interface", Japan. J. Appl. Phys. **59**, SAAC11 (2020).
- [150] M. A. El-Erian, "Navigating the new normal in industrial countries", Per Jacobsson Foundation Lecture (2010).